ORIGINAL ARTICLE

Insights into application of novel citric acid modified *Saccharum munja* biosorbent for facile removal of fuchsin basic dye, crystal violet dye and copper metal ion: statistical modelling, kinetics, thermodynamics and equilibrium studies

Nishita Sharma[1] · Aruna Yadav[1] · Sarita Yadav[1] · Sonika Singh[1] · Ashok K. Sharma[2] · Surender Kumar[1]

Abstract

With the recent rapid growth of the dyeing industries, extensive water contamination driven on by heavy metals and synthetic organic dyes has become more and more dangerous. Herein, we focused on adopting an adsorptive approach and designing of highly efficient and novel citric acid–modified *Saccharum munja* (CA-SM) with substantially dispersed adsorption sites for the adsorption of organic dyes and heavy metal. The physicochemical properties of as-synthesised biosorbent were explored by characterising with field emission scanning electron microscopy (FESEM), energy-dispersive X-ray spectroscopy (EDX), Fourier transform infrared spectroscopy (FTIR), X-ray diffraction (XRD) and differential scanning calorimetry (DSC). Further, Box-Behnken design under response surface methodology was employed to optimise the various parameters like pH, dosage and concentration. The model was found to be significant, reproducible and highly precise. The thermodynamics study revealed the adsorption process to be endothermic and spontaneous in nature. Moreover, the isotherm data was well fitted with Langmuir model for crystal violet (CV) and fuchsin basic (BF) dyes, while copper (Cu^{2+}) adsorption was best fitted with Temkin model. The maximum monolayer adsorption capacity for CV, BF and Cu^{2+} was 265.95, 229.88 and 10.054 mg/g respectively. Pseudo-second-order kinetic model was found to be the best representatives for all the contaminants. Furthermore, hydrogen bonding, pi-pi interactions and electrostatic interactions governed an important role towards the adsorption mechanism. Overall, this work involves the utilisation of citric acid–modified *Saccharum munja* as a novel and sustainable biosorbent for removal of dyes and heavy metal.

Keywords Adsorption · Crystal violet · Fuchsin basic · Heavy metal · Biosorbent · *Saccharum munja*

1 Introduction

Increasing contamination of global water resources and challenges in rapid treatment and detection of the wide range of contaminants impose significant strains on public health. According to World Health Organization report, only 25% of the world's population is privy to safe drinking water [1]. Water pollution is mainly caused by the industries that discharge dyes, heavy metals, pharmaceutical effluents and a variety of other organic contaminants [2]. These conventional and emerging contaminants pose consequent jeopardising threats to ecosystems and human health due to their persistence, toxicity and potential for bioaccumulation. In recent years, the escalating concern over environmental pollution has prompted the research for effective and eco-friendly remediation strategies.

Conventional methods, such as chemical deposition, ion exchange, coagulation-flocculation, photocatalytic degradation, membrane separation, adsorption and adsorptional-photocatalytic remediation [3–9], have been utilised to eradicate the dyes and heavy metal pollutants from water resources. Most of these methods have shown limitations in terms of efficiency, cost and environmental impact. Consequently, researchers have turned their attention towards

✉ Surender Kumar
 skaushik@cblu.ac.in

1 Department of Chemistry, Chaudhary Bansi Lal University, Bhiwani 127031, Haryana, India

2 Department of Chemistry, Deenbandhu Chhotu Ram University of Science and Technology, Murthal, Sonepat 131039, Haryana, India

sustainable and greener solutions that utilise biodegradable materials capable of efficiently sequestering these pollutants from contaminated water sources. Considering this aspect, adsorption using biomass-based adsorbents in raw or modified form is one of the simple strategies that has piqued the interest of researchers due to its low cost, unique chemical composition, abundant availability, ease of design, renewable nature and high efficiency when compared to other methods [10–13]. These biomass-based adsorbents have cellulose, hemicelluloses and lignin as their main constituents. They may also contain additional functional groups, such as hydroxyl, carbonyl, carboxyl, aldehyde, phenolic and/ or ether groups, which can interact with wastewater pollutants through a wide range of selective binding mechanisms [14]. However, the adsorption efficiency of raw biomass wastes is often lower than those of synthetic commercial adsorbents [15]. As a result, various physical and chemical treatment procedures using organic compounds (citric acid, tartaric acid, malic acid, methanol), oxidising agents (H_2O_2, $KMnO_4$, formaldehyde), bases (NaOH, Na_2CO_3, $Ca(OH)_2$), organic and mineral acids (HCl, H_2SO_4, HNO_3, acetic acid) and other chemicals (epichlorohydrin, $SOCl_2$, $ZnCl_2$) have been employed to improve the sorption characteristics of raw biomass [16–18]. Among these modifiers, citric acid modified biomasses have emerged as a promising, economic and eco-friendly approach to address the growing concerns of water pollution. Importantly, such a renewable and sustainable approach aligns with the principle of circular economy and green chemistry. Different biomass such as red seaweed [19], watermelon shell [20], rice straw [21], soyabean straw [22], soyabean hulls [23], kenaf core fibres [24], pine cone [25], wheat straw [26], peanut shell [27], corncob [28], pine sawdust [29], *Ceiba Pentandra* hulls [30] and coffee grains [31] have been modified with citric acid and studied for the removal of contaminants from wastewater. Further, as per prior reports, citric acid is a non-toxic crosslinking agent or chelator that can be esterified with hydroxyl groups under heat to generate a new material surface, enhancing metal ion or dye adsorption capability [27, 29]. However, continuous research and development are still needed to fully explore the potential of CA-modified biosorbents and integrate them into mainstream water purification technologies.

Cationic dyes, BF and CV are notorious for their carcinogenic and death-defying nature and have been identified as more toxic than anionic dyes, with relatively high tinctorial values (< 1.0 mg/L) [32]. Even at low concentrations, these chemical dyes pose a serious risk to marine life as well as human health. CV, a triarylmethane dye, is used to prevent and suppress the growth of the fungal infection. It can be used as a bacteriostatic agent and as an active element in Gram's stain. CV has liability for causing moderate eye irritation, causing painful sensitisation to light [33, 34]. Basic fuchsin dye is also a triarylmethane dye that is inflammable

in nature and has anaesthetic, antibacterial and fungicidal characteristics. It is frequently employed as a colorant in textile and leather goods, as well as in the staining of collagen and muscle and mitochondria, as well as tubercle bacteria [35–37]. Due to its properties of poor biodegradation, toxicity, carcinogenicity and unsightliness, the removal of both CV and BF from wastewater systems is of great concern and should be tested and employed promptly. Cu^{2+} is hazardous to aquatic life even at low concentrations in natural water and can cause abnormalities with the hepatic, renal, capillary and central nervous systems [38]. The highest permitted content of Cu^{2+} in drinking water, according to Environmental Protection Agency (EPA) and World Health Organization (WHO) recommendations, is 2 and 1.3 mg/L, respectively [39]. Furthermore, EPA has issued a copper limit of 0.25 mg/L for industrial effluent discharged to surface water [22]. The more hazardous oxidation state of copper is the divalent state [40]. If people are exposed to copper concentrations above 1.3 mg/L even for short periods of time, various diseases and disorders such as liver damage, stomach and intestinal problems, Wilson disease and insomnia may cause [41, 42]. Thus, the removal of dyes and heavy metals from wastewater is crucial because they constitute a major threat to both human and the environment.

Saccharum munja (SM) is a widespread perennial grass of the Poaceae family that is resistant to drought and covers an area of around 14.0 million square kilometres on Earth. It is primarily found in arid locations [43]. The plant has a potent regenerative capability and was primarily utilised for the extraction of munj fibre; however, with the growing popularity of synthetic fibres, the intended use of this plant has gradually diminished, resulting in overgrowth [44]. Therefore, SM is presently a waste biomass that farmers periodically burn, causing atmospheric pollution. SM contains 35.1% cellulose, 38.9% hemicellulose and 17.9% lignin, which provides a variety of functional groups for interaction with adsorbates [45, 46], since these lignocellulosic materials comprise hydroxyl groups on their surface and these functional groups can also be changed to improve the adsorption effectiveness of native SM for removal of water contaminants [47]. Therefore, in this study, we have chemically functionalised the native SM for the efficient elimination of contaminants from aqueous solution.

On the basis of literature review, we found that various biomass has been modified chemically to introduce surface functional groups for the enhanced adsorption of dyes and heavy metals. However, among various modifications, the use of citric acid is a comparatively greener and economic approach for modification of biomass. Also, different biomass has been modified with citric acid for the removal of contaminants. On critical analysis of these reports, we found that the scheme adopted for the modification is not completely optimised. Secondly, the effect of binder amount

on the chemical modification is not addressed well. Thus, considering these gaps, in the present work, novel citric acid–modified SM biosorbents have been synthesised by varying the amount and concentration of binder KH_2PO_4 and CA respectively, while the best formulation thus obtained was further utilised. To the best of our knowledge, there is no report on the chemical functionalisation of SM with citric acid for the efficient elimination of crystal violet dye, fuchsin basic dye and copper metal ion from aqueous solution. Herein, carboxyl groups were introduced into the cellulosic material through the esterification of citric acid which resulted in enhanced adsorption performance as well as its stability. Furthermore, the modification of SM with CA is an ecologically friendly process as well as it also avoids secondary contamination [48]. The optimisation of factors affecting the adsorption efficiency of CA-SM was carried out statistically using BBD-RSM design. The complicated interactions occurring between pH, dosage and concentration were evaluated systematically in order to achieve the highest contaminant removal by carrying out 17 tailored experiments[49]. The reproducibility, adequacy, precision and significance of the model were predicted in terms of statistical coefficients like coefficient of variance, adequate precision value, model F value and p-value. 2-D and 3-D plots were also examined to study the mutual interactions of the affecting parameters. Further, the kinetics and thermodynamics of the process were evaluated along with the isotherm studies to explore the underlying adsorption process mechanism and spontaneity of the overall process. Conclusively, the primary goals of this research are to (i) investigate a novel biosorbent and assess its efficacy in eliminating dyes and heavy metals from wastewater; (ii) produce and characterise carboxylic acid–functionalised biosorbent that meets 4-E strategy, i.e. environmental benign, easy to prepare, efficient and economical; (iii) elucidate its biosorption process through an investigation of kinetic, thermodynamics, equilibrium and statistical modelling; and (iv) investigate the adsorption mechanism involved in adsorption process. Overall, the present work provides a sustainable approach for treating dyes and heavy metal–contaminated water efficiently and would significantly contribute to the reduction of carbon footprints.

2 Materials and methods

Saccharum munja (SM) plant stems were collected from region near Chaudhary Bansi Lal University, Bhiwani, India, located at geographical coordinates of 28°86′N latitude and 76°9′E longitude. All the reagents and chemicals utilised were of high quality and analytical grade. Fuchsin basic (BF, Basic Fuchsin, $C_{20}H_{20}ClN_3$, M.W.=337.84g/mol), copper(II) chloride ($CuCl_2 \cdot 2H_2O$, 99%), hydrochloric acid (HCl), nitric

acid (HNO_3), sulphuric acid (H_2SO_4), sodium chloride (NaCl, 99.9%), sodium hydroxide (NaOH, 98%) and acetone (99.5%) were purchased from Sisco Research Laboratories Pvt. Ltd.; crystal violet (CV, methyl violet 10B, $C_{25}H_{30}ClN_3$, M.W. 408g/mol) was obtained from Himedia Laboratories Pvt. Ltd., while potassium dihydrogen orthophosphate (KH_2PO_4, >99%) and citric acid (99.5%) were procured from Fischer Scientific India Pvt. Ltd.

## 2.1 Preparation and optimisation of CA-modified native SM

The stems of SM were cut into small pieces, peeled off to remove the outer hydrophobic layer and subjected to washing with distilled water repetitiously to remove dust and impurities. It was oven-dried at 50°C, grinded, sieved through the 120 BSS mesh sieve and stored in an air-tight container and denoted by native SM as given in Scheme 1.

For the modification of native SM with CA and to study the effect of binder, KH_2PO_4, on the infusion of CA on the biomass surface, two trials were conducted as per scheme I and IV given in the Table 1. Further, six different schemes (II to VII) were followed by varying the concentration of CA from 0.05 to 1 M. The ratio of CA to binder was kept constant for the schemes II–VII. Briefly, 0.5 g of native SM was stirred in 50 mL of CA and KH_2PO_4 solutions as provided in the Table 1 for 1 h at room temperature. The dispersion was kept in oven at 150°C for complete evaporation of the solvent. As, the prepared CA-modified biosorbents, after successful esterification, was repeatedly washed with distilled water until neutral pH was obtained. Further, TDS of the filtrate was also checked to ensure the absence of soluble contents of SM into the aqueous phase/filtrate. The obtained CA-modified adsorbents were dried, grinded, sieved and used in powdered form after treatment.

Further, the percentage removal of the BF (50 ppm), CV (50 ppm) and Cu (25 ppm) was analysed by adding 0.01 g, 0.01 g and 0.02 g of the adsorbents obtained as per schemes given in Table 1 to 10 mL of solution volume. It was observed that maximum removal was obtained with the adsorbent prepared as per scheme IV, which was denoted by CA-SM and used for further studies.

2.2 Characterisation of adsorbent

The modification of native SM with CA and infused physicochemical characteristics were analysed through various characterisation techniques like FESEM, EDX, FTIR, XRD and DSC. The porosity and changes in surface morphology of the adsorbent before and after adsorption was observed by FESEM (7610F Plus, JEOL). EDX (Ametak) was employed to configure the elemental composition of the adsorbent. Moreover, FTIR analysis (using Frontier, Perkin Elmer
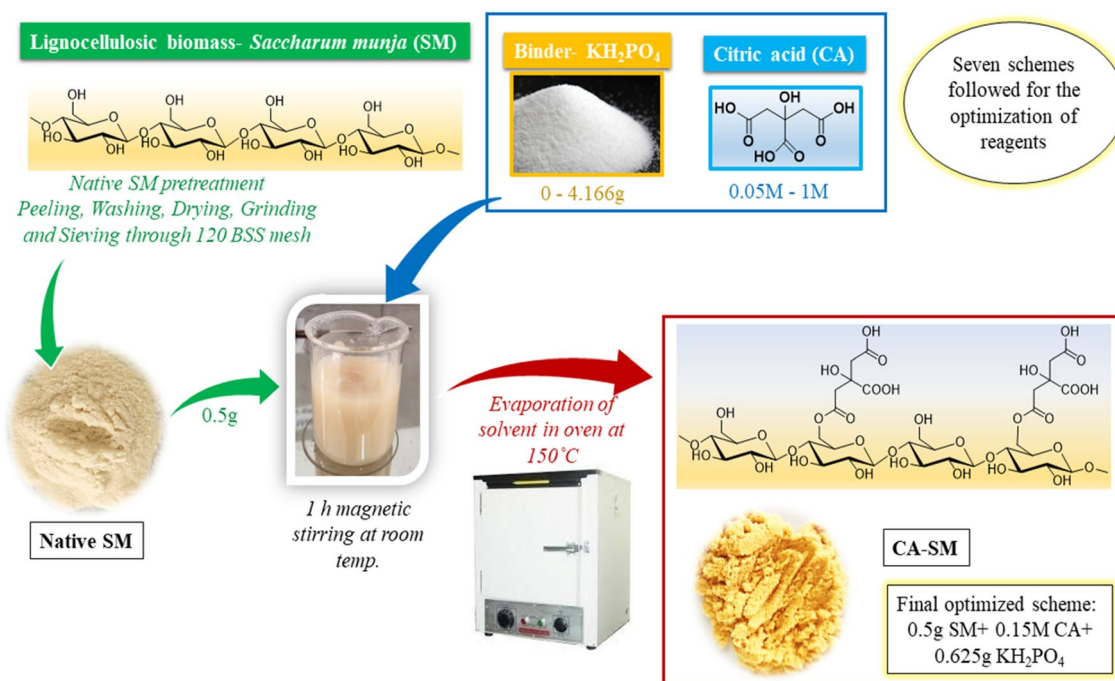
Scheme 1 Preparation of CA-SM biosorbent

Table 1 Schemes for the optimisation of reagents

Scheme no.	Amount of native SM (g)	Concentration of CA (50 mL)	Amount of KH$_2$PO$_4$ (g)
I	0.5	0.15 M	0
II	0.5	0.05 M	0.2083
III	0.5	0.10 M	0.416
IV	0.5	0.15 M	0.625
V	0.5	0.2 M	0.833
VI	0.5	0.5 M	2.083
VII	0.5	1 M	4.166

spectrometer) was observed to ascertain the chemical functional groups on the surface of the adsorbent with a scanning range of 4000–400 cm^{-1}. The crystal phase structure analysis of the adsorbent was carried out on a Rigaku X-Ray Powder Diffractometer Miniflex-600 (using CuKα radiation with wavelength 1.5 A°) in the range 5° to 80° (2θ) with a scanning rate of 2 degrees per minute. Further, the thermal stability and enthalpy changes were performed on a TA Instruments Waters make DSC, Q-10 model with a heating rate of 10 °C/min.

2.3 Batch adsorption studies

Separate stock solutions of BF (1000 mg/L), CV (1000 mg/L) and Cu (500 mg/L) were prepared by dissolving a requisite amount of BF dye, CV dye and CuCl$_2$ respectively in distilled water, which was further diluted to obtain different concentrations involved in the study. The pH of the dyes and heavy metal solutions was adjusted by using 0.1M NaOH and 0.1M HCl solutions. In the present study, to optimise and evaluate the effect of interacting factors like pH, concentration and dosage, Box-Behnken design (BBD) under response surface methodology (RSM) was adopted. The experimental model of BBD was based on three coded factors named as concentration (A), dosage (B) and pH (C), and the % removal was opted as the response of the design. For the dye solutions, the experimental model under BBD design consists of 17 customised setups involving the varying range of initial concentration (50–500 mg/L), CA-SM dosage (0.01g–0.03g/10mL) and pH of dye solution (2–11). However, the interacting parameters for Cu consists of initial concentration (5–50 mg/L), CA-SM dosage (0.02–0.06g/20mL) and pH of Cu solution (2–8) involving 17 different experimental setup. The contact time for RSM modelling for both BF and CV dyes was 10 min while the contact time for Cu was 30 min. Further, the analysis of variance (ANOVA) was checked for finding out the significance of the most suitable model for each of dyes and heavy metal. In a typical procedure, a known amount of adsorbent was stirred on a temperature-controlled magnetic stirrer with a definite volume of dye (10 mL) or heavy metal (20mL) solution with a specified pH for a fixed time, and the % removal as a response was noted.

The initial and residual concentration of dyes in the solutions before and after the adsorption was quantitatively analysed by using a UV-Visible spectrophotometer (Systronics, 117) and measuring the absorbance of BF and CV at a wavelength of 546 nm and 582 nm respectively. The concentration of Cu in the solution was determined by using atomic adsorption spectrophotometer (GBC 932 plus) at a wavelength of 222.6 nm. The following equations (1–3) [33, 45, 50] were employed for calculation of percentage removal and adsorption capacity of dyes and heavy metal:

$$\% \, \boldsymbol{Removal} = \frac{(C_o - C_e)}{C_o} \times 100 \tag{1}$$

$$\text{At equilibrium, } \boldsymbol{Adsorption \, Capacity}, \, \boldsymbol{q_e(mg/g)} = \frac{(C_o - C_e) \times V}{M} \tag{2}$$

$$\text{At anytime, } t, \, \boldsymbol{Adsorption \, Capacity}, \, \boldsymbol{q_t(mg/g)} = \frac{(C_o - C_t) \times V}{M} \tag{3}$$

where C_o (mg/L) is the initial concentration; C_e (mg/L) is the equilibrium concentration, C_t (mg/L) is the concentration at time t; M is the mass of adsorbent in g and V is the volume of solution in L.

The point of zero charge (pH_{pzc}) was calculated by following the pH-drift method as earlier reported in the literature [51]. Briefly, 0.15 g of CA-SM was added in 50 mL solution of 0.01 N NaCl with initial pH ranging from 2 to 12, stirred continuously for 24h, filtered, and the final pH of the solution was noted.

For exploration of kinetic study of adsorption for dyes, 0.01g of CA-SM was dispersed in 10 mL of 75mg/L dye solution with a time period of 1 to 60 min while 0.04g of CA-SM was added in 20 mL of 25mg/L Cu solution with a time range varying from 1 to 120 min. Further, the isotherm study for dyes (BF and CV) was conducted by varying the concentration from 50 to 500 mg/L with CA-SM dosage of 0.01g/10mL for a contact time of 10 min, while isotherm study for Cu involved the range of concentration (5–50 mg/L) with CA/

dosage of 0.04 g/20 mL for a contact time of 30 min. The thermodynamics study was carried out in the temperature range of 25–60 °C (dye concentration = 75 mg/L with CA-SM dosage of 0.01 g/10 mL for 10 min and Cu concentration = 25 mg/L with CA-SM dosage of 0.04 g/20 mL for 30 min).

3 Results and discussion

3.1 Optimisation of CA-modified adsorbent and evaluation of pH_{pzc} of CA-SM

Native SM was modified by varying the concentrations of CA solution and respective amount of binder under the schemes I to VII as given in Table 1. In order to optimise the best modified adsorbent, the % removal of dyes (BF and CV) and Cu was evaluated by using native SM and the adsorbents obtained from different schemes. It was observed that native SM showed a removal of 74.10%, 92.36% and 46.35%, while the adsorbent prepared under the scheme IV showed a removal of 95.98%, 98.17% and 68.07% for BF, CV and Cu respectively. By comparing the % removal of all the three contaminants by the prepared adsorbents, it was analysed that the adsorbent obtained from scheme IV gives the best result which was utilised for further studies. The % removal of native SM and other adsorbents for BF, CV and Cu is represented in Fig. 1a.

The pH_{pzc} is the value of pH at which the surface of biomass behaves as neutral in terms of charge distribution. The pH_{pzc} of CA-SM was calculated to be 3.47 by using pH-drift method as depicted in Fig. 1b. The incorporation of –COOH groups was confirmed by the resonating values of pH_{pzc} (3.47) of the adsorbent and pK$_a$ value (3) of carboxyl group. At pH >3, –COOH groups were present in –COO$^-$ form while at pH <3, protonated form as –COOH was present. Moreover, the surface of CA-SM as a whole carried a positive charge at pH <3.47 and negative charge was more dominating at pH >3.47.

Fig. 1 **a** Optimisation results for native SM and CA-modified adsorbents and **b** pH_{pzc} of CA-SM
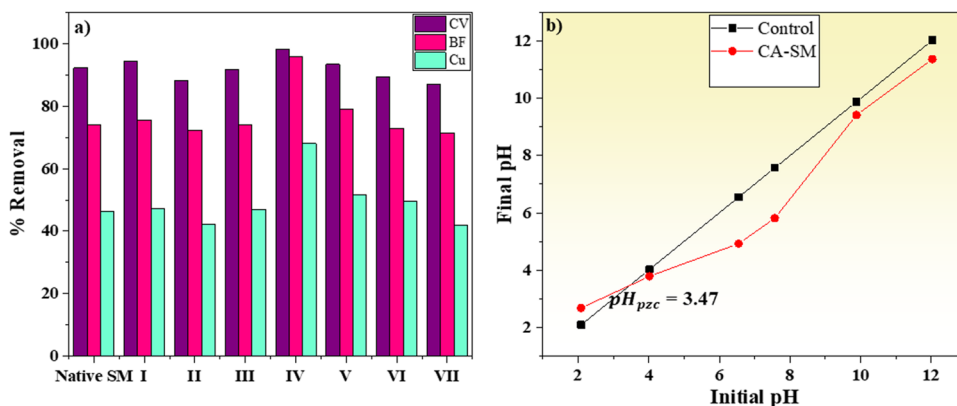
3.2 Characterisation studies

3.2.1 FESEM analysis

The structural and surface morphological characteristics including porosity and roughness of native SM and CA-SM were analysed with FESEM as shown in Fig. 2a–d. Fig. 2a clearly demonstrates the porous structure of native SM having an oval opening. The surface of native SM was also analysed at different magnifications that shows the smooth as well as vibrant porous surface texture. Moreover, the incorporation of CA onto native SM surface enhanced the surface roughness as shown in Fig. 2c. The CA-SM showed a highly varied surface with an apparent significant variation in pore sizes (Fig. 2d) and surface morphology. The increased roughness as well as incorporation of CA onto native SM surface resulted in more interaction with dyes and heavy metal.

3.2.2 EDX

EDX elemental mapping was employed to analyse the elemental composition of adsorbents. The EDX data of native SM and CA-SM is depicted in Fig. 3a and b respectively. By analysing the weight % age of different elements in Fig. 3a and b, it was noticed that weight % of oxygen got enhanced in CA-SM as compared to native SM which was attributed to incorporation of oxygenated functional groups onto native

SM surface. This observation is directly responsible for the carboxylic modification of native SM surface with CA.

3.2.3 FTIR

FTIR spectra of native SM, CA-SM, BF-loaded SM, CV-loaded SM and Cu-loaded SM were analysed as given in Fig. 4. The major peaks observed in native SM were at 1034 cm^{-1}, 1098 cm^{-1}, 1159 cm^{-1}, 1239 cm^{-1}, 1321 cm^{-1}, 1371 cm^{-1}, 1509 cm^{-1}, 1603 cm^{-1}, 1634 cm^{-1}, 1728 cm^{-1}, 2893 cm^{-1} and 3345 cm^{-1}. The peaks between 1000 and 1200 cm^{-1} corresponds to fingerprint region of the cellulosic group [25]. The peak obtained at 1239 cm^{-1} is attributed to ether linkage between lignin and carbohydrates [52]. The band at 1510 cm^{-1} is accompanied with stretching of aromatic rings [27]. The peak at 2900 cm^{-1} was due to the C–H asymmetrical stretching vibration of methyl groups on the surface [27]. The broad band obtained at 3345 cm^{-1} was due to stretching vibrations of O–H stretching groups from cellulose, hemicellulose and lignin; and the sharp peak at 1035 cm^{-1} was due to hemicellulose C–O stretching [22, 53]. After modification of native SM with CA, the position of most of the peaks was the same with slight variations in peak intensity. The major change was associated with the peak at 1728 cm^{-1} in native SM that got shifted to 1722 cm^{-1} with an enhanced peak intensity indicating the successful esterification of native SM with CA [21]. Moreover, two new peaks were observed in CA-SM at 1204 cm^{-1} and 1426 cm^{-1} where the peak at 1204 cm^{-1} corresponds to C–O

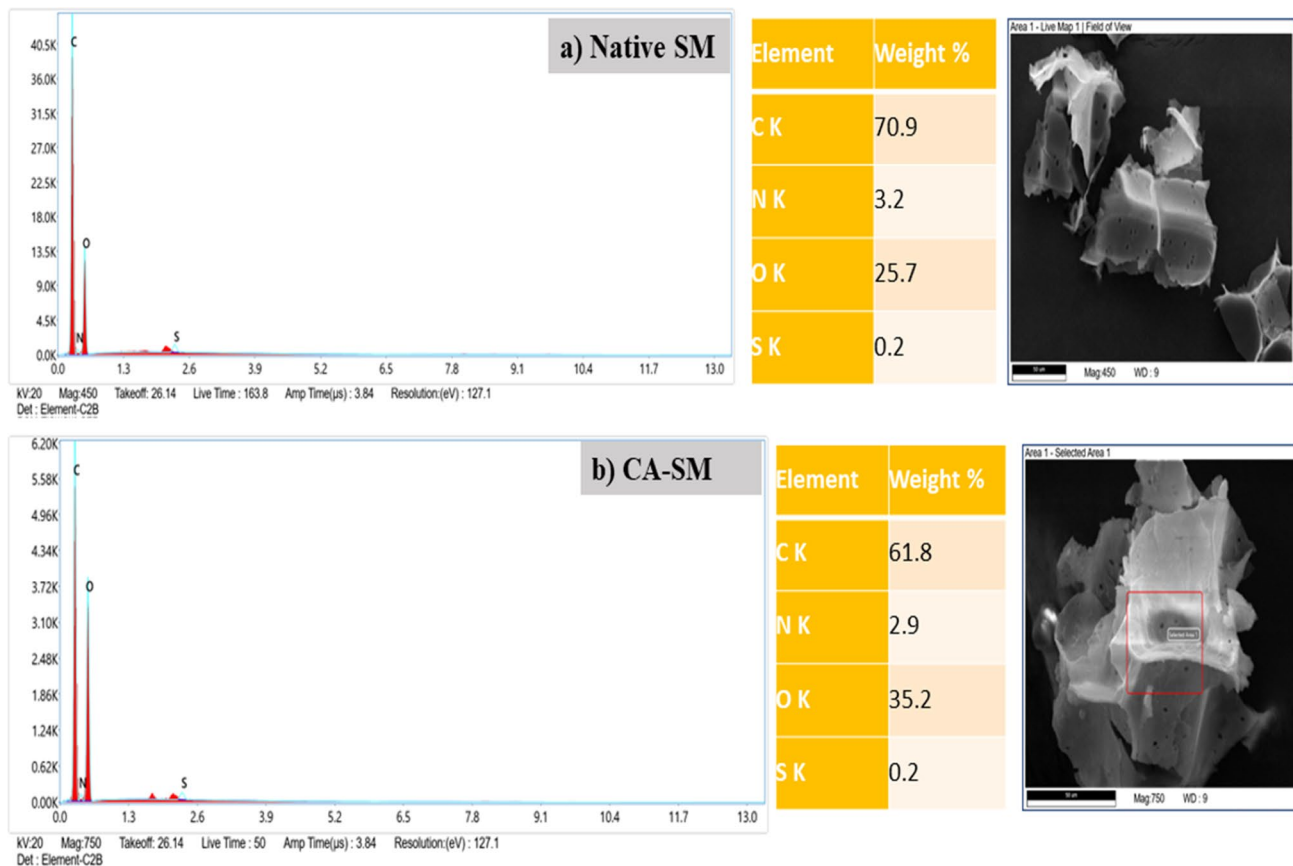**Fig. 2** FESEM images of native SM (**a–b**), CA-SM (**c–d**)
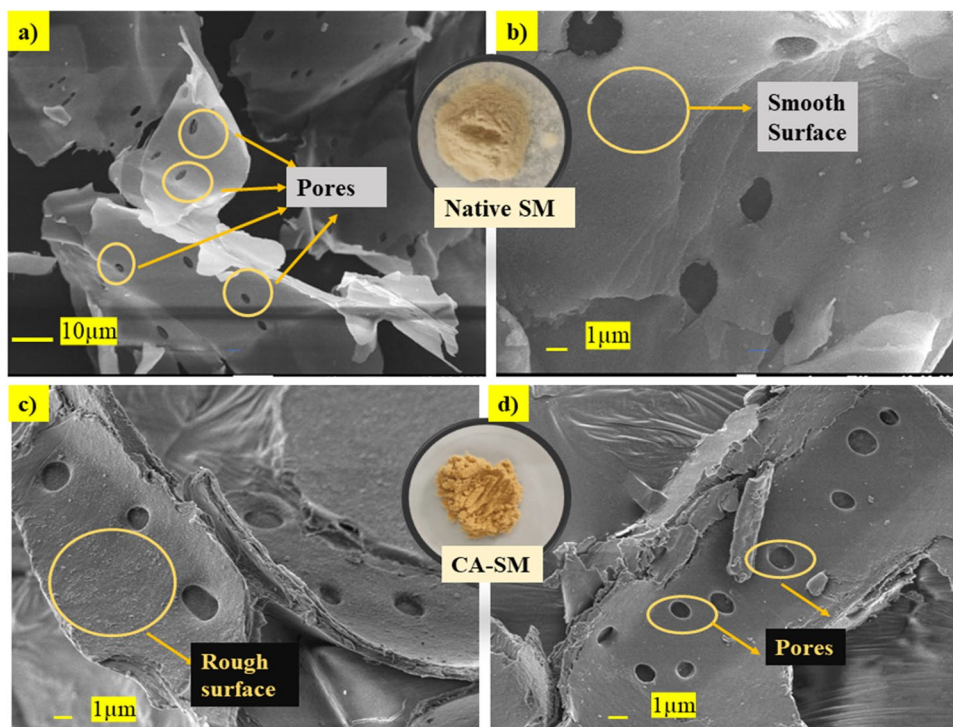
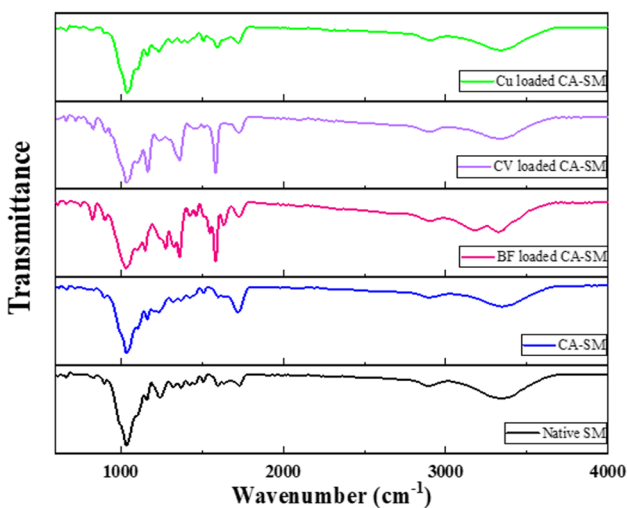**Fig. 3** EDX analysis of native SM (**a**) and CA-SM (**b**)

**Fig. 4** FTIR spectra of native SM, CA-SM, BF-loaded CA-SM, CV-loaded CA-SM and Cu²⁺ loaded CA-SM

stretching band of ester and the peak at 1426 cm⁻¹ corresponds to OH stretching of carboxylic acid that played a good role in dye adsorption. The BF-loaded CA-SM showed

a characteristic peak at 3189 cm⁻¹ due to N–H stretching involved during hydrogen bonding. Further, a pronounced enhancement of the C=C band of the aromatic rings at 1584 cm⁻¹ in FTIR of BF-loaded CA-SM and CV-loaded CA-SM suggests a significant change in polarity of new molecule due to adsorption of these dyes on CA-SM surface [28]. However, in FTIR of Cu-loaded CA-SM, a broader band was observed at 3345 cm⁻¹ indicating the involvement of hydroxyl groups in binding of Cu metal ions and the intensity of peak at 1722cm⁻¹ also got reduced due to the interactions of carboxylic functional groups with Cu metal ions.

3.2.4 XRD

The XRD of native SM and CA-SM as depicted in Fig. 5a was analysed to discuss various aspects associated with the crystallinity of the material. The XRD patterns of both native SM and CA-SM showed the main peaks at 2θ=21.7° which is due to crystallinity of cellulose showing the (002) crystal plan; and the secondary solder peaks at 2θ=16.5° is attributed to the amorphous part of cellulose [54]. The peak at 2θ=35° corresponds to cellulosic portion of the biosorbent. The relative presence of similar peaks for native SM

Fig. 5 **a** XRD of CA-SM and native SM, **b** DSC curve for CA-SM
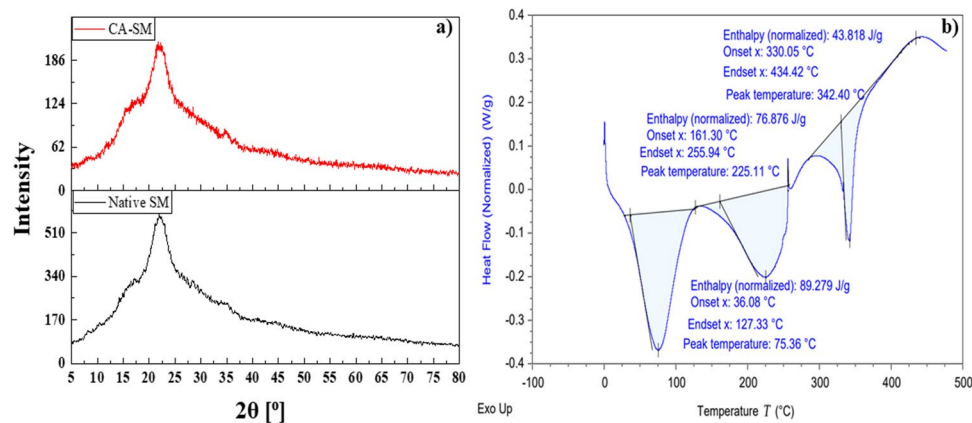
and CA-SM demonstrates that the esterification introduced no specific changes to SM surface and incorporation of CA did not damage the crystal organisation of cellulose after esterification [55, 56]. The sharp peak corresponds to the crystallinity of the material. The absence of the sharp peak indicates the amorphous nature of native SM and CA-SM suggesting that dyes and metal ion could more easily penetrate into the rough surface of the adsorbent. Moreover, the reduced crystallinity can be ascribed to the insertion of the grafted chains of CA onto the native SM backbone, which may lead to breaking of hydrogen bonding in the CA-SM structure, resulting in an amorphous structure [30].

3.2.5 DSC

The DSC curve for CA-SM is depicted in Fig. 5b and three endothermic peaks at 75.6°C, 225.11°C and 342.40°C were observed. The first endothermic peak at 75.6°C corresponds to desolvation of water molecules present in CA-SM [57]. The absence of melting point peak of CA at 160°C gives an evidence for absence of free CA in the biosorbent [58]. Moreover, the peaks observed at 225.11°C and 342.40°C were due to thermal decomposition of hemicellulose and cellulose structure present in CA-SM respectively [55, 59].

3.3 RSM modelling with CA-SM

RSM is a statistical and mathematical modelling tool to evaluate the effect of various interacting factors and optimise the most preferred conditions in order to maximise the particular response of the design. The suitability of RSM can also be ensured to diagnose the reproducibility and significance of the experiment in terms of best suited model following the central-composite design, BBD, three-level factorial design, hybrid design etc. Also, the 2D diagnostic plots of RSM are a promising tool to check

the resonance between the actual and predicted value of response, and to observe the trend of studentised residuals. Moreover, ANOVA gives a statistical approach to the model and resolves about the adequacy and validity of the model in terms of regression coefficients.

3.3.1 BBD design

In the present study, BBD design was implemented to study impact of interactional behaviour of the three independent variables [concentration (A), dosage (B) and pH (C)] on the % removal (Response) of the dyes and heavy metal. The design was checked for the fitting of linear, quadratic and cubic model; but the quadratic model was found to be the best suited in all cases. BBD-RSM design matrix along with actual and predicted value of response (% removal) is given in Table 2 (for BF and CV dye) and Table 3 (for Cu^{2+}). Further, ANOVA was employed to explain the interaction between various independent variables in terms of second order polynomial equation. The BBD-RSM regression model equations obtained for calculation of % removal in terms of coded factors are given in Eqs. (4, 5, 6) for BF, CV and Cu^{2+} respectively, where positive sign before the terms signifies the synergistic effect while the negative sign corresponds to antagonistic effect of coded factors A, B and C towards the % removal of dyes and heavy metal [60].

$$\% \text{ Removal (BF)} = + 83.69 - 11.67 \times A + 5.35 \times B + 14.28 \times C$$
$$+ 2.25 \times A^2 - 0.23 \times B^2 - 5.96 \times C^2 + 4.27$$
$$\times A \times B + 6.16 \times A \times C - 4.26 \times B \times C$$
$$(4)$$

$$\% \text{ Removal (CV)} = + 92.78 - 8.05 \times A + 5.22 \times B + 8.43 \times C - 1.02$$
$$\times A^2 - 1.54 \times B^2 - 5.37 \times C^2 + 3.60 \times A \times B$$
$$+ 1.68 \times A \times C - 3.90 \times B \times$$
$$(5)$$

Table 2 BBD-RSM design matrix for BF and CV dye along with actual and predicted values of % removal

Standard order	A: concentration (ppm)	B: dosage	C: pH	% removal actual value (BF)	% removal predicted value (BF)	% removal actual value (CV)	% removal predicted value (CV)
1	175	0.02	6.5	84.14	83.69	92.68	92.78
2	175	0.03	11	94.58	92.88	96.94	95.61
3	300	0.03	6.5	84	83.67	89.46	90.98
4	175	0.01	2	51.92	53.62	67	68.33
5	300	0.01	6.5	65.7	64.43	73.48	73.35
6	175	0.02	6.5	85.19	83.69	93.93	92.78
7	50	0.02	11	99.35	99.78	99.98	101.18
8	175	0.01	11	91.46	90.70	92.65	92.97
9	175	0.02	6.5	82.83	83.69	91.24	92.78
10	175	0.02	6.5	84.96	83.69	93.67	92.78
11	175	0.03	2	72.06	72.82	86.88	86.56
12	300	0.02	11	86.72	88.76	88.64	88.44
13	300	0.02	2	48.31	47.88	69.43	68.23
14	50	0.01	6.5	95.98	96.31	98.17	96.65
15	50	0.02	2	85.57	83.53	87.49	87.69
16	50	0.03	6.5	97.18	98.45	99.76	99.89
17	175	0.02	6.5	81.35	83.69	92.37	92.78

Table 3 BBD-RSM design matrix for Cu along with actual and predicted values of % removal

Standard order	Factor A: concentration (mg/L)	Factor B: dosage (g)	Factor C: pH	Response: % removal actual value (Cu^{2+})	Response: % removal predicted value (Cu^{2+})
1	5	0.06	5	98.14	96.69
2	27.5	0.04	5	64.58	64.15
3	5	0.04	8	99.27	100.58
4	27.5	0.02	2	39.96	39.82
5	27.5	0.04	5	64.91	64.15
6	27.5	0.04	5	65.24	64.15
7	27.5	0.04	5	63.26	64.15
8	27.5	0.06	2	52.96	52.44
9	50	0.06	5	47.41	49.24
10	5	0.02	5	92.37	90.54
11	27.5	0.04	5	62.76	64.15
12	27.5	0.02	8	68.23	68.75
13	50	0.04	8	58.45	56.49
14	5	0.04	2	79.52	81.49
15	50	0.04	2	21.79	20.48
16	50	0.02	5	31.46	32.91
17	27.5	0.06	8	78.47	78.61

$$\% \text{ Removal (Cu)} = + \ 64.15 - 26.27 \times A + 5.62 \times B + 13.77 \times C$$
$$+ \ 4.02 \times A^2 - 0.83 \times B^2 - 3.42 \times C^2 + 2.55$$
$$\times A \times B + 4.23 \times A \times C - 0.69 \times B \times C$$

(6)

where A, B and C are linear coefficients; A^2, B^2 and C^2 are quadratic coefficients; and AB, AC and BC are the interacting coefficients.

Table 4 ANOVA results for quadratic model under BBD-RSM for removal of BF dye, CV dye and Cu^{2+}

Source	Sum of squares			DF	Mean square			F-value			Prob>F			
	BF	CV	Cu^{2+}		BF	CV	Cu^{2+}	BF	CV	Cu^{2+}	BF	CV	Cu^{2+}	
Model	3412.79	1571.73	7506.39	9	379.20	174.64	834.04	90.31	76.28	214.28	<0.0001	<0.0001	<0.0001	Significant
A	1089.28	518.26	5522.48	1	1089.28	518.26	5522.48	259.41	226.38	1418.79	<0.0001	<0.0001	<0.0001	
B	228.55	217.78	252.68	1	228.55	217.78	252.68	54.43	95.13	64.92	0.0002	<0.0001	<0.0001	
C	1631.63	568.01	1517.73	1	1631.63	568.01	1517.73	388.58	248.11	389.92	<0.0001	<0.0001	<0.0001	
A^2	21.35	4.39	68.17	1	21.35	4.39	68.17	5.08	1.92	17.51	0.0588	0.2085	0.0041	
B^2	0.22	9.97	2.89	1	0.22	9.97	2.89	0.053	4.36	0.74	0.8239	0.0753	0.4173	
C^2	149.48	121.49	49.14	1	149.48	121.49	49.14	35.60	53.07	12.62	0.0006	0.0002	0.0093	
AB	73.10	51.77	25.91	1	73.10	51.77	25.91	17.41	22.61	6.66	0.0042	0.0021	0.0365	
AC	151.66	11.29	71.49	1	151.66	11.29	71.49	36.12	4.93	18.37	0.0005	0.0618	0.0036	
BC	72.42	60.76	1.90	1	72.42	60.76	1.90	17.25	26.54	0.49	0.0043	0.0013	0.5068	
Residual	29.39	16.03	27.25	7	4.20	2.29	3.89							
Lack of fit	19.11	11.36	22.57	3	6.37	3.79	7.52	2.48	3.25	6.44	0.2006	0.1425	0.0519	Not Significant
Pure error	10.28	4.66	4.67	4	2.57	1.17	1.17							
Cor total	3442.18	1587.76	7533.63	16										

Table 5 Statistical model coefficients for BF, CV and Cu^{2+}

Model coefficients	BF	CV	Cu^{2+}
Std. dev.	2.05	1.51	1.97
C.V.	2.50	1.70	3.08
R-square	0.9915	0.9899	0.9964
Adj R-squared	0.9805	0.9769	0.9917
Pred R-squared	0.9065	0.8809	0.9511
Adeq precision	33.023	28.394	52.932

3.3.2 ANOVA results and adequacy of the model

The best suited quadratic model was statistically evaluated by ANOVA; and Fisher F-test and probability test were also analysed to check the suitability of the model. The results of ANOVA for BF, CV and Cu^{2+} are given in Table 4. The model F-values obtained for BF, CV and Cu^{2+} were 90.31, 76.28 and 214.28 respectively with a prob $> F$ value of < 0.0001 which indicates the model to be significant. The higher the F-value, the more suitable is the model to elucidate about the variations in the data and as a result, the actual values of significant terms are in closer vicinity of estimated values [61]. Analysing the F-value for model terms, it was observed the influence of independent factors decreased in the order as pH > concentration > dosage for all BF, CV and Cu^{2+}; i.e. pH is the most significant factor that affects the response of the model. Moreover, the lack of fit F-value for BF, CV and Cu^{2+} as 2.48, 3.25 and 6.44 indicates that lack of fit is not significant as compared to pure error. The prob $> F$-value of significant terms should be less than 0.05 while all the terms with values greater than 0.1000 of prob>F are not-significant. By examining all the interaction terms involved in the model, it was concluded that A, B, C, C^2, AB, AC and BC are the significant model terms for BF; A, B, C, C^2, AB and BC are the significant model terms for CV; and A, B, C, A^2, C^2, AB and AC are the significant model terms for Cu^{2+}. The more the number of significant model terms, the more reliable is the model.

Furthermore, other statistical parameters like coefficient of determination (R^2), predicted R^2, adjusted R^2, coefficient of variation, standard deviation and adequate precision were also analysed as shown in Table 5. The values of R^2 as 0.9915 (BF), 0.9899 (CV) and 0.9964 (Cu^{2+}) are close to 1 which shows that there exists a better correlation between actual and predicted values of the response. ANOVA suggested that there is a reasonable agreement between the adjusted R^2 and predicted R^2 values for BF (0.9805, 0.9065), CV (0.9769, 0.8809) and Cu^{2+} (0.9917, 0.9511) which proves the model to be highly significant and reliable. Moreover, the small values of standard deviation (BF =2.05, CV=1.51, Cu^{2+}=1.97) and coefficient of variation (BF=2.5%, CV=1.7%, Cu^{2+}=3.08%) reflect the

statistical reproducibility of the model. Typically, a value less than 10% for coefficient of variance is desirable for adequate reproducibility of the model which is in reasonable agreement with the present study [62]. The value of adequate precision (signal to noise ratio) should be greater than 4 in order to justify the adequacy of the signal. Herein, the adequate precision of 33.023, 28.394 and 52.932 for BF, CV and Cu^{2+} respectively shows that the models are reasonably good and adequate in prediction [63]. Therefore, all these models can be utilised for designing of navigate space.

The adequate approximation of the model to real system was further verified with the help of diagnostic plots for BF, CV and Cu^{2+} as depicted in Fig. 6. The normal plot of the residuals plotted between normal % probability and studentised residuals suggests that data points should form a straight line against a theoretical normal distribution. The more the aberration from the straight line, the more is the aberration from the normal distribution. It was analysed that the vicinity of all the data points to the straight line demonstrates the independence of the residuals [64]. Further, the plot of predicted values vs actual values depicted that there is a closer agreement between actual and predicted values

which ensures the experimental data to be an acceptable fit for the statistical validation [65].

3.3.3 Effect of variables and their interactions

The 3-D RSM plots for BF, CV and Cu^{2+} are shown in Fig. 7 that demonstrates the in-depth interaction of independent variables and the response (% removal) of the model. For the suggested models, pH is considered the most significant factor that strongly affects the removal efficiency of dyes and Cu^{2+}. It was observed that increase in pH from 2 to 11and 2 to 8 has a positive effect on the removal of dyes and Cu^{2+} respectively; i.e. adsorption of dyes and Cu^{2+} was favoured at higher pH due to electrostatic interactions arising between the negatively charged CA-SM surface and positively charged surface of cationic dyes (BF and CV) and Cu^{2+}. This behaviour of adsorbent surface is attributed to pH_{pzc} (CA-SM=3.47) which shows that at pH > pH_{pzc}, the surface of CA-SM would carry a net negative charge, and at pH < pH_{pzc}, the surface of CA-SM would be positively charged. In case of adsorption of Cu^{2+} on CA-SM surface, the negatively charged surface sites of the adsorbent will promote the uptake of Cu^{2+} ions at higher pH level
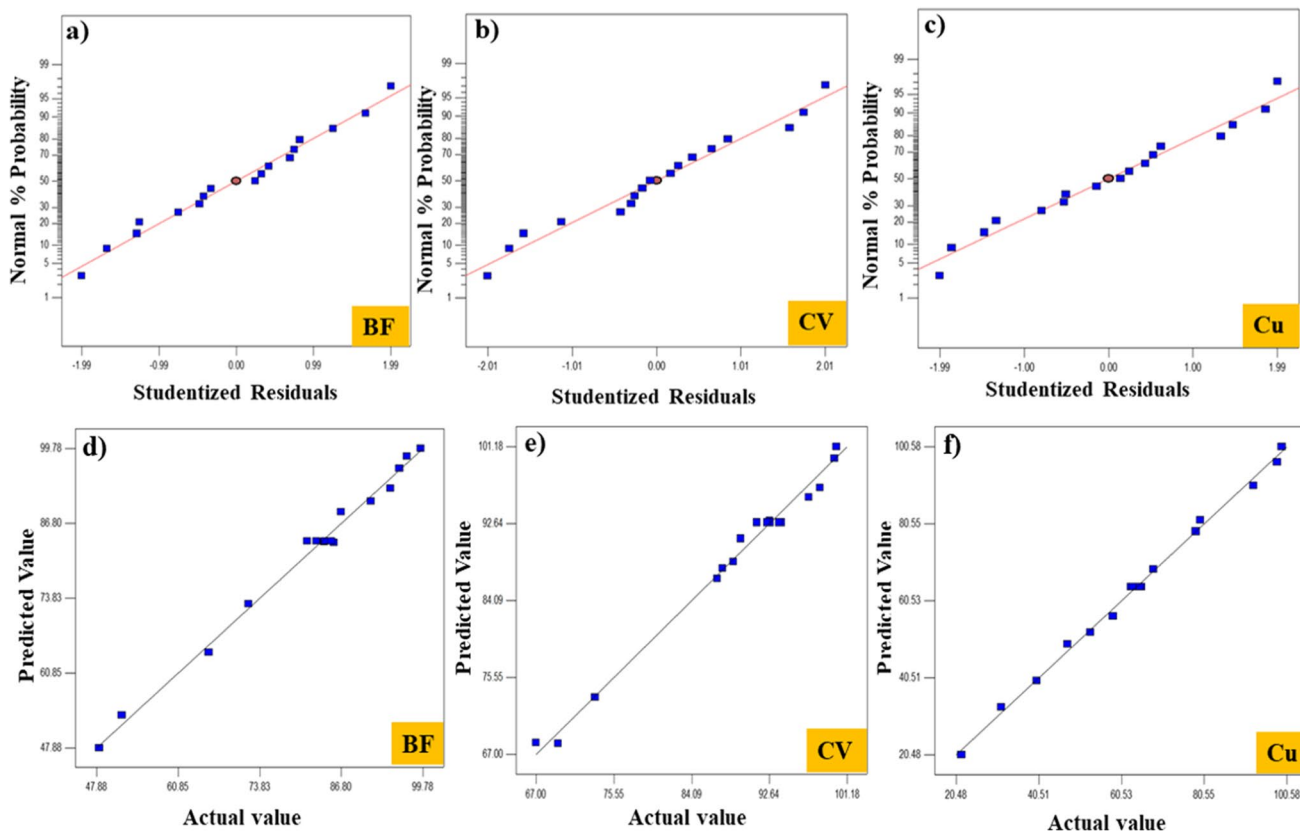
Fig. 6 **a–c** Normal plot of residuals BF, CV and Cu respectively; **d–f** diagnostic plot of predicted value vs actual value for BF, CV and Cu respectively
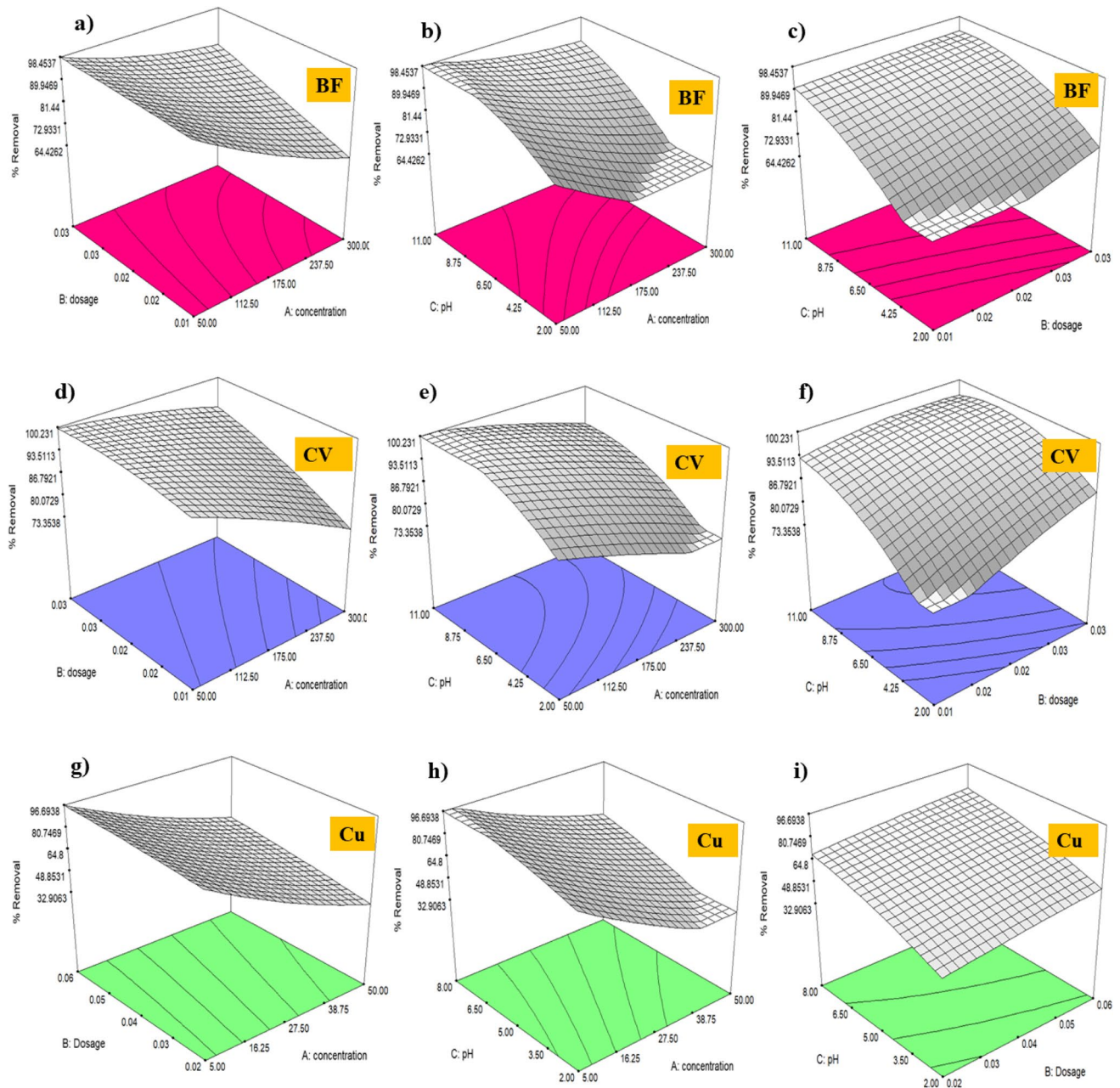
Fig. 7 The 3D RSM plots for BF (**a–c**), CV (**d–f**) and Cu²⁺ (**g–i**); and standard error plots for BF (**j–l**), CV (**m–o**) and Cu²⁺ (**p–r**)

till optimum (pH=6). Further, the removal of Cu^{2+} ions increased as a combined result of hydrolysis and adsorption which was also verified with the formation of white precipitates forming the colloidal complex [20]. Moreover, the removal of dyes and Cu^{2+} gets increased with increase in dosage of CA-SM which is due to availability of more active binding sites and greater surface area for adsorption; and the binding sites of the adsorbent becomes saturated at higher initial concentration; therefore, the dyes and Cu^{2+} uptake gets decreased with the increase in initial concentration [20]. Further, the impact of two interacting factors on the %

removal while keeping the other factors constant have been presented in the graphs depicted in Fig. 7a–i. The standard error plots for BF, CV and Cu^{2+} as given in Fig. 7j–r also show a good fit to quadratic model.

3.4 Kinetic study

The contact time has a significant relevance with the adsorption mechanism and adsorption efficiency of the adsorption process. An efficient adsorption process is allied with short contact time, faster rate of reaction and significant
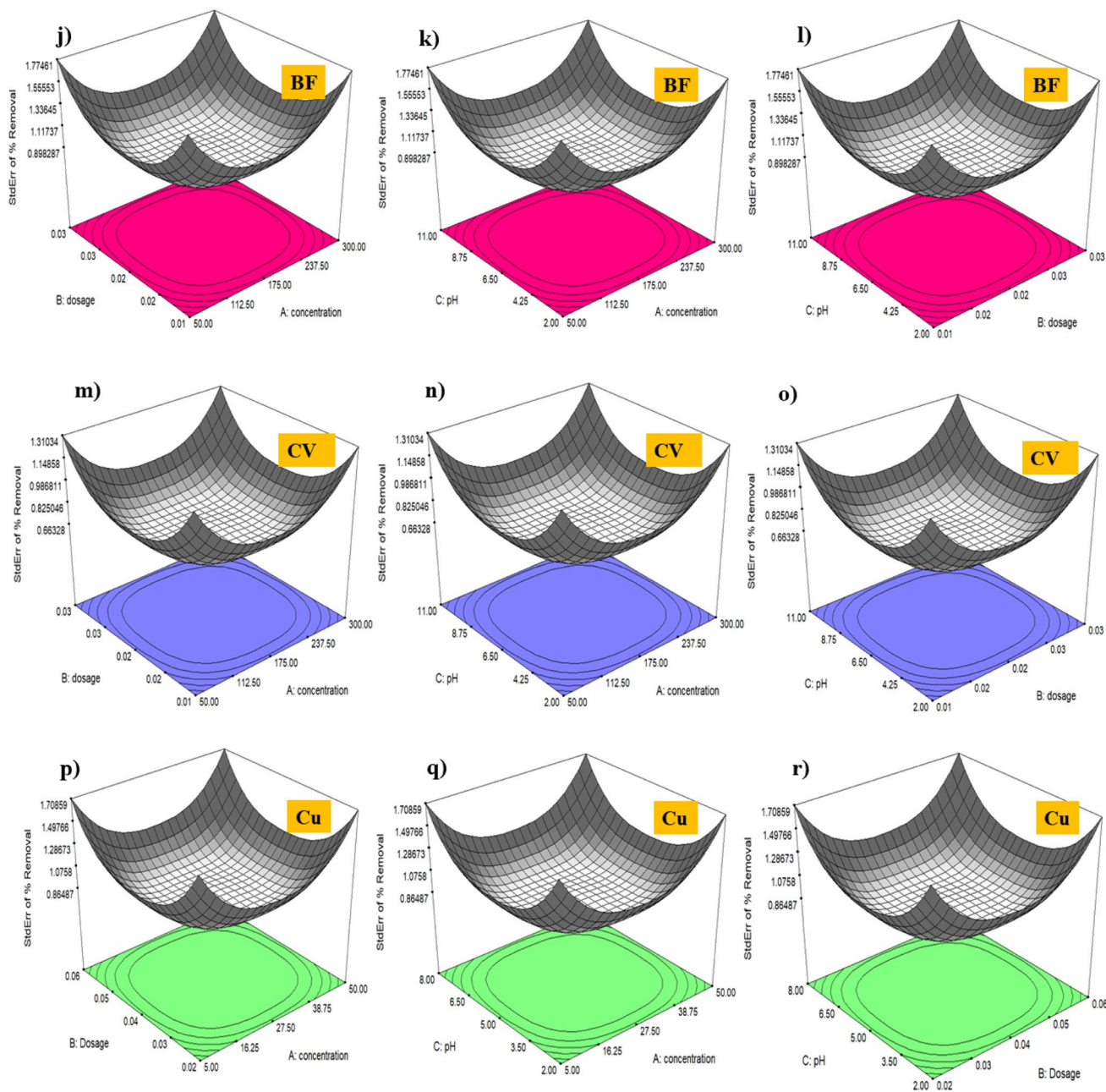
Fig. 7 (continued)

adsorption efficiency. Therefore, to predict and understand the underlying mechanism, the time-dependent experiments were performed. The rate-limiting step involved in the kinetics of adsorption process was determined by using different kinetic models as given in Eqs. 7–10 [11, 56, 66]:

3.4.1 Pseudo-first-order model

$$Ln(q_e - q_t) = Ln(q_e) - k_1 \times t \tag{7}$$

where k_1 (min^{-1}) is the pseudo-first-order rate constant; t (min) is the time; q_e (mgg^{-1}) is the adsorption capacity at equilibrium and q_t (mgg^{-1}) is the adsorption capacity at any time t.

3.4.2 Pseudo-second-order model

$$\frac{t}{q_t} = \frac{1}{k_2 q_e} + \frac{t}{q_e} \tag{8}$$

where k_2 (min^{-1}) is the pseudo-second-order rate constant; q_e (mgg^{-1}) is the adsorption capacity at equilibrium; t(min) is the time; q_t (mgg^{-1}) is the adsorption capacity at any time t.

3.4.3 Intraparticle diffusion model

$$q_t = k_{in}t^{1/2} + c \tag{9}$$

where q_t (mgg^{-1}) is the adsorption capacity at any time t; k_{in} (mgmin$^{-1/2}$g^{-1}) is intraparticle diffusion rate constant and c (mgg^{-1}) is the thickness of boundary layer; t(min) is the time.

3.4.4 Elovich model

$$q_t = \frac{1}{\beta}Lnt + \frac{1}{\beta}\text{Ln}(\alpha\beta) \tag{10}$$

where q_t (mgg^{-1}) is the adsorption capacity at any time t, t (min) is the time, α (mgg^{-1}min^{-1}, degree of adsorption) is the primary rate of adsorption and β is the desorption parameter associated with characterisation of degree of chemisorption and activation energy.

The obtained experimental data was checked for fitting with all the kinetic models and the graphs were plotted as depicted in Fig. 8. Moreover, all the parameters associated with kinetic models are given in Table 6 for comparative study of models. Based on the model R^2 value, it was observed that the adsorption kinetics of BF, CV and Cu^{2+} were more fitted with the pseudo-second-order kinetic model which highlights the importance of chemisorption as the rate-limiting step and governs the involvement of physico-chemical interactions between adsorbent and adsorbate [67]. The value of calculated q_e(mgg^{-1}) for BF, CV and Cu^{2+} were 70.028, 72.326 and 9.503 respectively which were in a good correlation with the experimental q_e(mgg^{-1}).

3.5 Isotherm study

The impact of initial concentration of BF (50–500 mg/L), CV (50–500 mg/L) and Cu^{2+} (5–50 mg/L) on the adsorption capacity of CA-SM was explored in order to envisage the nature of favourable adsorption and the allied interactions of adsorbate-adsorbent. The batch experiment study was performed at neutral pH and 298 K temperature with CA-SM dosage and contact time of 0.01 g/10 mL and 10 min; and 0.04g/20 mL and 30 min for dyes (BF and CV) and Cu^{2+} respectively. Further, the experimental data was fitted with various adsorption isotherm models to obtain the equilibrium adsorption parameters and understand the distribution of adsorbate molecules on CA-SM surface. Fig. 9 shows the different isotherm plots for BF, CV and Cu^{2+}, and the modelled parameters calculated from these plots are given in Table 7.

3.5.1 Langmuir isotherm model

Langmuir isotherm model corresponds to monolayer homogeneous adsorption. The maximum adsorption capacity of adsorption process was calculated by plotting a graph between $1/q_e$ vs $1/C_e$ using the linear form of Langmuir model as given in Eq. 11 [63].

$$\frac{C_e}{q_e} = \frac{C_e}{q_{max}} + \frac{1}{k_L q_{max}} \tag{11}$$

where C_e (mgL^{-1}) is the dye concentration at equilibrium, q_e (mgg^{-1}) is the adsorption capacity at equilibrium, q_{max} (mgg^{-1}) is the maximum adsorption capacity of adsorbent; k_L (Lmg^{-1}) is the Langmuir adsorption equilibrium constant which is related to free energy of adsorption.

3.5.2 Freundlich isotherm model

Freundlich model corresponds to multilayer heterogeneous adsorption. Freundlich parameters were calculated by plotting a graph between Lnq_e vs LnC_e using the following equation [68];

$$Lnq_e = Lnk_F + \left(\frac{1}{n}\right)LnC_e \tag{12}$$

where q_e (mgg^{-1}) is the adsorption capacity at equilibrium, k_F ((mgg^{-1}) (Lmg^{-1})$^{1/n}$) is the Freundlich parameter that represents the adsorbed quantity and n is the Freundlich constant related to index of adsorption intensity or surface heterogeneity.

3.5.3 Temkin isotherm model

Temkin model is based upon the assumption that heat of adsorption decreases as the coverage and interaction of adsorbate over adsorbent increases; and the underlying interactions between adsorbate and adsorbent cannot be ignored during adsorption process [32]. A graph between q_e vs LnC_e was plotted by using the following equation [69]:

$$q_e = \frac{RT}{b}Lnk_t + \frac{RT}{b}LnC_e \tag{13}$$

where k_t (Lmol^{-1}) is the Temkin equilibrium binding constant (relates to the maximum binding energy); b (Jmol^{-1}),R (8.314 JK^{-1}mol^{-1}) and T (298 K) are heat of adsorption, universal gas constant and temperature respectively; B_T= RT/b is the Temkin constant which is a dimensionless quantity.

3.5.4 Dubinin-Radushkevich isotherm model

Dubinin-Radushkevich (DR) model expresses the adsorption on a heterogeneous surface having a Gaussian energy distribution. The physical and chemical nature of adsorption
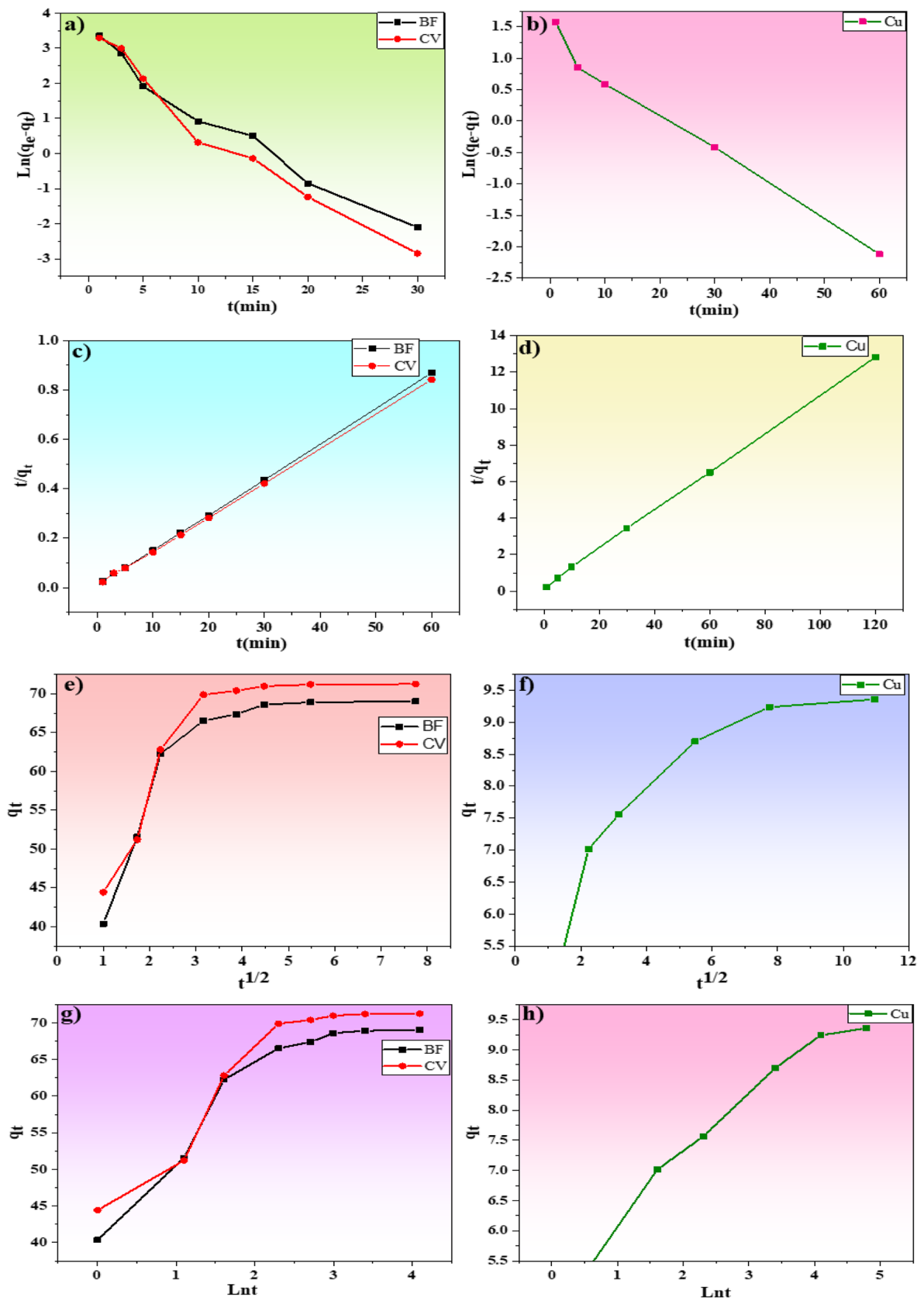
Fig. 8 Kinetic plots for pseudo-first-order model (**a**–**b**), pseudo-second-order model (**c**–**d**), intraparticle diffusion model (**e**–**f**) and Elovich model (**g**–**h**)

Table 6 Different kinetic model parameters for removal of BF, CV (initial conc.= 75 mg/L, adsorbent dosage=0.01g/10 mL, contact time=1–60 min) and Cu^{2+} (initial conc. = 25 mg/L, adsorbent dosage=0.04g/20 mL, contact time= 1–120 min) at 298K

Kinetic models	Parameters	BF	CV	Cu^{2+}
Pseudo-first-order model	q_e(mgg^{-1})	23.815	25.234	3.774
	k_1(min^{-1})	0.18562	0.21519	0.0581
	R^2	0.97154	0.96743	0.98062
Pseudo-second-order model	q_e(mgg^{-1}) calculated	70.028	72.306	9.503
	q_e(mgg^{-1}) experimental	69.03	71.264	9.359
	k_2(min^{-1})	0.0215	0.0217	0.0534
	R^2	0.99987	0.99975	0.99982
Intraparticle diffusion model	k_{in}(mgmin$^{-1/2}$g^{-1})	3.64332	3.71404	0.42043
	c(mgg^{-1})	48.30015	50.23041	5.58691
	R^2	0.58385	0.59852	0.73663
Elovich model	α(mgg^{-1}min^{-1})	34.704	28.194	147.651
	β	0.1378	0.13699	0.97973
	R^2	0.84267	0.84179	0.95454

can be assessed in terms of mean free energy. Various DR model parameters were calculated by using the following equation and plotting a graph between ***Lnq_e* vs *ε*².**

$$Lnq_e = Lnq_D - \beta\varepsilon^2 \qquad (14)$$

where q_e (mgg^{-1}) is the adsorption capacity at equilibrium, q_D(mgg^{-1}) denotes the DR model maximum adsorption capacity; ε is the Polanyi potential, $\varepsilon = RT\left(1 + \frac{1}{C_e}\right)$; β (mol^{2}KJ^{-2}) is the average energy of adsorption and the mean free energy is $E = \frac{1}{\sqrt{2\beta}}$; if $E < 8$ KJmol^{-1}, adsorption is dominated by physical forces and if 8 KJmol$^{-1} < E < 16$ KJmol^{-1}, the adsorption is dominated by the chemical forces [69].

Based on the correlation coefficient, it was observed that the best fitted models were Langmuir > Freundlich > Temkin > DR, Langmuir > Freundlich > Temkin > DR and Temkin > Langmuir > Freundlich > D-R for BF, CV and Cu^{2+} respectively. It indicates that Langmuir model is suitable for understanding the adsorption process related with dyes, while Temkin model gives better understanding towards Cu^{2+} adsorption. The suitability of Langmuir model for dyes assigns that the adsorption is monolayer and homogeneous. All the adsorption sites are singly occupied and possess the similar energy for binding with the adsorbate molecules. The value of q_{max} obtained from Langmuir model was 229.88 mgg^{-1}, 265.95 mgg^{-1} and 10.054 mgg^{-1} for BF, CV and Cu^{2+} respectively. The k_L value for Cu^{2+} (1.255) > CV (0.0569) > BF (0.0392) indicates the more stability of Cu^{2+}-CA-SM complex as compared to CV-CA-SM complex which is higher than BF-CA-SM complex [69]. Moreover, on the basis of Langmuir model, the favourability of adsorption process is judged in terms of separation factor, R_L, as given in Eq. 15 [19]

$$R_L = \frac{1}{(1 + k_L C_o)} \qquad (15)$$

which indicates that the adsorption is favourable for $0 < R_L < 1$, unfavourable for $R_L > 1$, irreversible for $R_L = 0$ and linear for $R_L = 1$. Based on the experimental results, R_L values are 0.347–0.050, 0.260–0.033 and 0.137–0.015 for BF, CV and Cu^{2+} respectively that validates the highly favourable nature of the adsorption process. Moreover, Freundlich model was analysed in terms of heterogeneity factor which suggests that the adsorption process is favourable if $1/n$ value is less than 1 which correlates with the experimental results as $1/n$ value is less than 1 for all cases. The more is the vicinity of $1/n$ value to 1, the more is the heterogeneity of the surface [36]. Furthermore, the higher the value of k_F, the more is the adsorption efficiency for the adsorbate which concludes that adsorption efficiency shows an order as CV > BF > Cu^{2+} [54]. Temkin model helps in calculating the binding energy of adsorption process and ascertain about the electrostatic interactions between the adsorbate and adsorbent [56]. However, the DR model showed the lowest compatibility in comparison to other models in all cases. The low value of mean free energy E (KJmol^{-1}) (0.1299, 0.1957 and 2.442 for BF, CV and Cu^{2+} respectively) deduced from DR model proposes that the adsorption is physical in nature.

3.6 Thermodynamics study

The thermodynamics associated with the adsorption of BF, CV and Cu^{2+} on CA-SM surface was analysed by carrying out the adsorption experiments in the temperature range of 298–333 K. Different thermodynamic parameters like Gibbs free energy, enthalpy and entropy change were investigated to check out the feasibility, spontaneity and enthalpy of the adsorption process as given in Table 8. Based on experimental results, a graph between LnK_d vs 1/T (Vant-Hoff plot) was plotted as demonstrated in Fig. 10 and the slope and
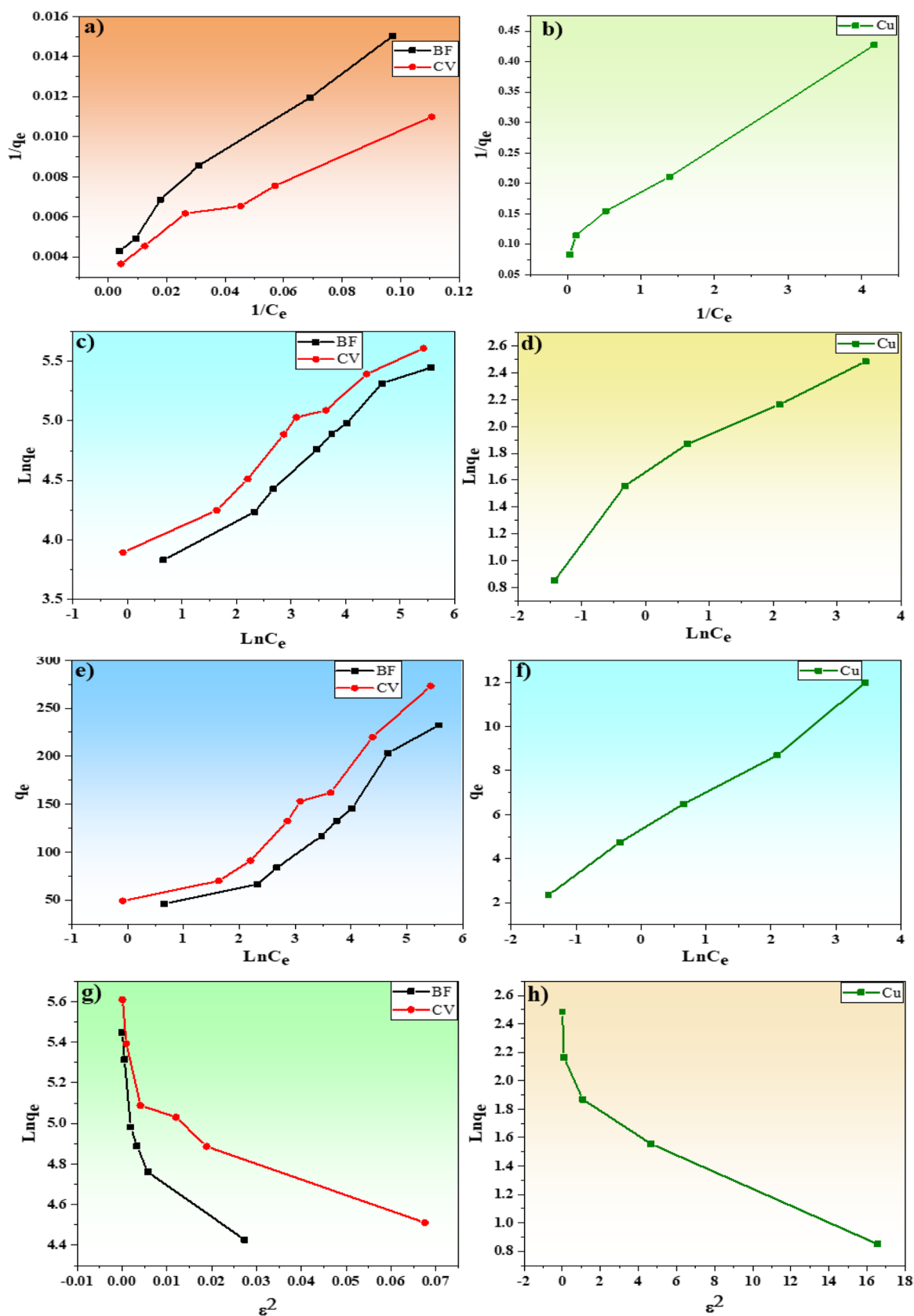
Fig. 9 Isotherm plots for Langmuir model (**a–b**), Freundlich model (**c–d**), Temkin model (**e–f**) and DR model (**g–h**)

Table 7 Different isotherm model parameters for removal of BF, CV (Initial Conc.= 50–500 mg/L, adsorbent dosage = 0.01g/10 mL, contact time= 10 min) and Cu^{2+} (Initial Conc.= 5–50 mg/L, adsorbent dosage = 0.04g/20 mL, contact time= 30 min) at 298 K

Isotherm models	Parameters	BF	CV	Cu2+
Langmuir model	q_{max}(mgg^{-1})	229.88	265.95	10.054
	k_L(Lmg^{-1})	0.0392	0.0569	1.255
	R^2	0.98486	0.98024	0.99233
Freundlich model	k_F((mgg^{-1}) (Lmg^{-1})$^{1/n}$)	33.843	47.379	4.509
	$1/n$	0.357	0.336	0.313
	R^2	0.97945	0.97118	0.93468
Temkin model	k_t(Lmol^{-1})	0.772	1.563	14.805
	b(Jmol^{-1})	60.480	57.569	1295.88
	B_T	40.965	43.036	1.91188
	R^2	0.91223	0.92839	0.99376
DR model	q_D(mgg^{-1})	174.58	202.71	8.65
	β(mol^{2}KJ^{-2})	29.61924	13.05305	0.08379
	E (KJmol^{-1})	0.1299	0.1957	2.442
	R^2	0.68723	0.75589	0.8735

Table 8 Thermodynamic parameters for the removal of BF, CV (initial conc.= 75 mg/L, adsorbent dosage = 0.01 g/10 mL, contact time= 10 min) and Cu^{2+} (initial conc.= 25 mg/L, adsorbent dosage = 0.04 g/20 mL, contact time= 30 min)

Adsorbate	Thermodynamic parameters				
	ΔG(KJmol^{-1})			ΔH	ΔS
	298 K	303 K	313 K	(KJmol^{-1})	(Jmol^{-1}K^{-1})
BF	−4.507	−6.855	−9.985	42.1268	156.492
CV	−6.313	−8.736	−11.966	41.8117	161.495
Cu	−0.169	−0.713	−1.438	10.6315	36.2465
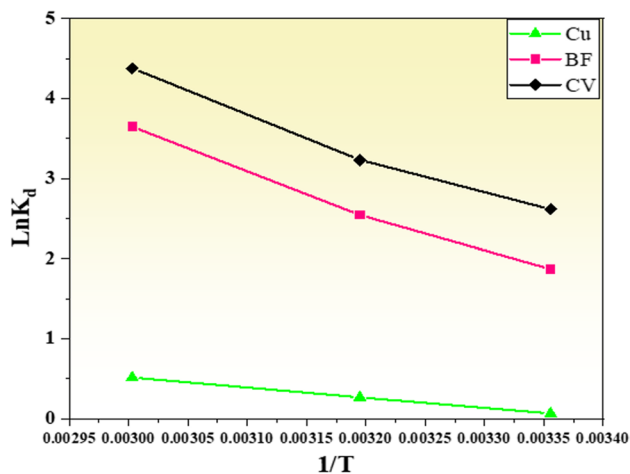
Fig. 10 Vant-Hoff plot for BF, CV and Cu^{2+} removal

intercept obtained from the graph were used to compute the thermodynamic modelled parameters by using the following equations [56, 70, 71]:

$$\Delta G = -RTLnK_d \tag{16}$$

$$\Delta G = \Delta H - T\Delta S \tag{17}$$

$$LnK_d = \frac{\Delta S}{R} - \frac{\Delta H}{RT} \tag{18}$$

where $K_d = \frac{q_e}{C_e}$ is thermodynamic equilibrium constant, T (K) is the absolute temperature at which the adsorption experiment was performed, R (8.314JK^{-1}/mol) is the universal gas constant, ΔH is the enthalpy change, ΔS is the entropy change and ΔG is the Gibbs free energy change.

The ΔG value in all the cases is negative and less than −20 KJ/mol suggesting the adsorption process to be spontaneous and physically controlled associated with electrostatic interactions [67]. Further, the decrease in ΔG value with the increase in temperature from 298 to 333 K proposes that rising temperature is favourable for adsorption indicating the process to be endothermic which is also certified by the positive value of ΔH (KJmol^{-1}) as 42.1268, 41.8117 and 10.6315 for BF, CV and Cu^{2+} respectively. The increase in temperature provides the enhanced kinetic energy of dyes molecules and heavy metal, and also reduces the viscosity of the solution that results in more diffusion of these molecules in the pores of the adsorbent and hence favours the adsorption process [72]. Moreover, the positive values of ΔS (Jmol^{-1}K^{-1}) as 156.492, 161.495 and 36.2465 for BF, CV and Cu^{2+} respectively indicate the expansion in randomness that may arise due to irregularity infused on adsorbent-adsorbate interface via adsorption.

3.7 Adsorption mechanism

The underlying adsorption mechanism involving the interactions between adsorbent and adsorbates was proposed

through the combined analysis of the results of batch adsorption studies, characterisation and theoretical simulations. The batch adsorption studies revealed the significant role of pH of solution in determining the adsorption efficiency. The adsorption of positively charged cationic dyes and heavy metal ion was favoured at pH>pH_{pzc} of CA-SM, due to the electrostatic interactions occurring between the positively charged adsorbates and the negatively charged adsorbent surface functional groups. Further, adsorption of BF, CV and Cu^{2+} at pH<pH_{pzc} of CA-SM evidences the involvement of other interactions such as H-bonding and pi-pi apart from electrostatic interactions. However, drastic changes in percentage removal of adsorbates with change in pH were observed, which indicates that electrostatic interactions are of much importance than other interactions. Another important aspect in the adsorption mechanism is the affinity order. From the adsorption capacity values, the observed trend for the cationic dyes is CV>BF. This can be explained on the basis of structure of dyes, where CV dye contains tertiary amine group while the BF dye contains primary amine group. Since tertiary amine is more basic than primary, hence the positive charge on nitrogen atom is more stable in the case of CV dye than that of BF. Hence, CV dye due to more basicity can show better electrostatic interaction with the adsorbent surface.

Adsorption of Cu^{2+} on the other hand showed a different trend. The RSM studies revealed that the percentage removal of Cu^{2+} increased constantly with the increase in the pH of solution from 2 to 8. This shows that apart from electrostatic interactions, precipitation at higher pH also governs the adsorption process. As per prior reports, Cu^{2+} ion exists in equilibrium with $Cu(OH)^{+}$ ion at pH 2–6.3 [22]. Further increase in pH results in the precipitation of Cu^{2+} in the form of $Cu(OH)_2$ which limits the interaction and sorption by the biosorbent [73]. Thus, at higher pH, the overall increase in Cu^{2+} removal was observed as a combined effect of precipitation as well as adsorption as shown in Fig. 11.

4 Comparison with other adsorbents

The comparison of the maximum monolayer adsorption capacity obtained by the Langmuir Isotherm model of various reported adsorbents and CA-SM is given in Table 9 that indicates the efficient adsorption potential of CA-SM and proves it to be a potential candidate for removal of dyes and heavy metal.

5 Conclusion and future perspectives

In the present work, we have developed a CA-modified SM biosorbent with abundant surface functionalities via a green, one pot, economic and facile approach. The synthesised biosorbent characterised with FESEM, FTIR,
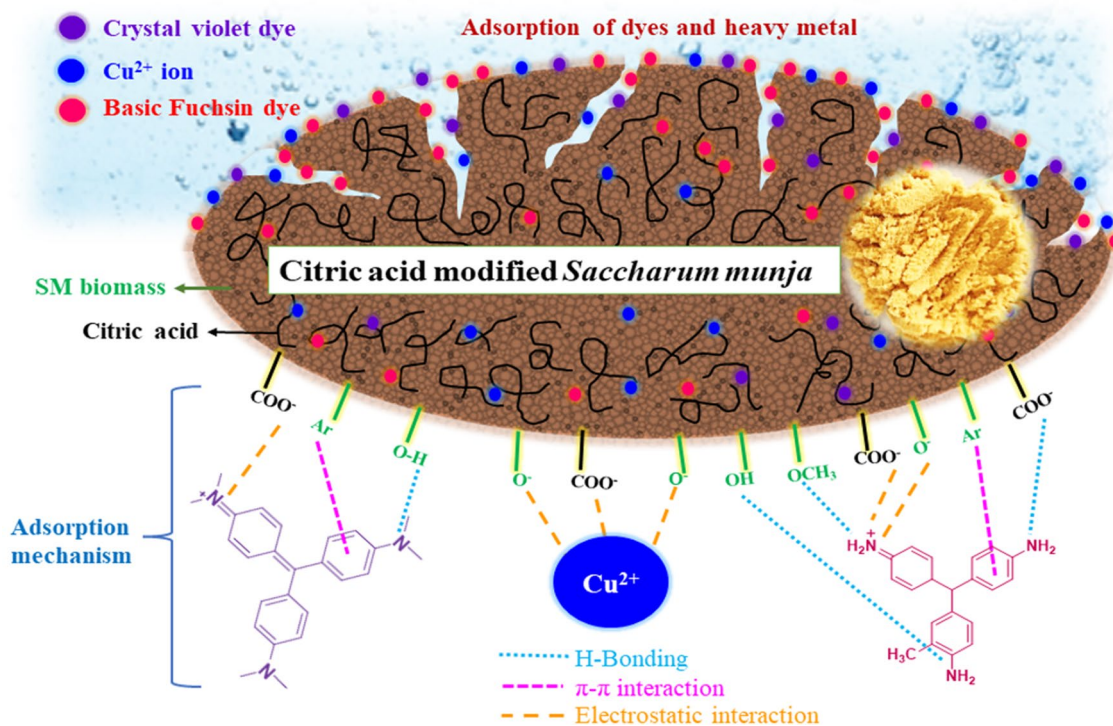

Fig. 11 Adsorption mechanism of dyes (BF and CV) and heavy metal (Cu) on CA-SM surface

Table 9 Comparison of q_{max} obtained from Langmuir model of CA-SM for BF, CV and Cu^{2+} with other adsorbents

Biosorbent	Contaminant removed	q_{max} (mg/g)	Reference
Calcined mussel shells	BF	141.65	[35]
HCl-treated malted sorghum mash	BF	58.48	[74]
Euryale ferox Salisbury seed shell	BF	19.48	[36]
CA-modified red seaweed	CV	217.38	[19]
Soyabean straw	Cu^{2+}	5.40	[75]
Wheat shell	Cu^{2+}	8.3	[76]
Pacara earpod tree (*Enterolobium contortisiliquum*)	BF	177.084	[77]
Ironwood (*Caesalpinia leiostachya*)	BF	136.526	[77]
Citrullus lanatus seed powder	CV	48.13	[78]
Citrullus lanatus seed powder	BF	44.26	[78]
Starch composite with peanut hull	CV	101.5	[79]
Pineapple leaf powder	CV	78.22	[80]
Citric acid–functionalised brown algae	CV	279.14	[81]
Citric acid–modified acacia leaves	CV	337.83	[82]
Citric acid–functionalised Acacia pods	CV	300.92	[83]
Banana peels	Cu^{2+}	4.75	[84]
Activated poplar sawdust	Cu^{2+}	9.24	[85]
CA-SM	CV	265.95	**This study**
CA-SM	BF	229.88	**This study**
CA-SM	Cu^{2+}	10.054	**This study**

XRD, EDX and DSC for studying the physicochemical features. Densely charged groups of CA-SM with massive accessibility were responsible for the enhanced adsorption of cationic dyes (CV and BF) and Cu^{2+} ion. Batch adsorption studies were carried out statistically using BBD-RSM design, where the model *F* values obtained for BF, CV and Cu were 90.31, 76.28 and 214.28 indicating the significance the model. The response of the model was influenced by the parameters in the order pH>concentration>dosage for all the three adsorbates as evaluated from the *F*-values. Moreover, the small values of standard deviation (1.51–2.05) and coefficient of variation (1.7–3.08%) reflected the adequacy and statistical reproducibility of the model with high adequate precision (28.394–52.932). 2-D and 3-D RSM plots were evaluated for examining the mutual interactions of parameters affecting the response. Further, the adsorption followed the pseudo-second-order model, while the thermodynamic studies reflected the endothermic, spontaneous and physisorption nature of adsorption for CV, BF and Cu. The experimental data was fitted with Langmuir, Freundlich, Temkin and D-R model, where the dyes CV and BF best followed the Langmuir model, while Cu^{2+} best followed the Temkin model. The maximum monolayer adsorption capacity of CA-SM for CV, BF and Cu^{2+} were 265.95, 229.88 and 10.054 mg/g respectively. The R_L<1 validated the favourable nature of adsorption. The biosorbent was able to completely remove the dyes and heavy metals from aqueous solution mainly through electrostatic, H-bonding, pi-pi interactions and precipitation. The affinity of CA-SM towards CV was found greater than BF under similar conditions due to its high basicity. Overall, the findings of present study will contribute towards the advancement of ecofriendly and efficient technologies that can mitigate the harmful impacts of water contaminants paving the way towards the cleaner and healthier future. The future scope of this study involves the application of biomass-based adsorbents for the adsorptive removal of dyes, heavy metals, antibiotics and pesticides. The multicomponent study for the removal of contaminants will be explored in order to attain a more practical and sustainable approach. Moreover, regeneration studies of adsorbents for the removal of contaminants are crucial for ensuring the sustainability and efficiency of the treatment process. The regeneration studies mainly comprises of effectiveness assessment (changes in the adsorption capacity/efficiency), regeneration method optimisation (selection of most suitable regenerating agent/eluent), economic viability (cost-effectiveness of regeneration process), environmental impact, long-term performance (multiple adsorption desorption cycles), compatibility with real-world effluent, scalability and practicality and characterisation of regenerated adsorbent by techniques like XRD, FTIR and FESEM. Considering the vital importance of regeneration studies,

our future work will be focussed on in-depth analysis of regeneration of spent CA-SM, and its application for the pilot-scale investigations on real-world effluent.

Declarations

Ethical approval It is stated that the present study does not involve any human or animal object.

Competing interests The authors declare no competing interests.

References

1. Xiao W, Jiang X, Liu X et al (2021) Adsorption of organic dyes from wastewater by metal-doped porous carbon materials. J Clean Prod 284:124773. https://doi.org/10.1016/j.jclepro.2020.124773

2. B R V, Barman P, Kadam R, Kumar A (2022) Lignin-based adsorbent for effective removal of toxic heavy metals from wastewater. Emergent Mater 5:923–943. https://doi.org/10.1007/s42247-021-00311-5

3. Sharma G, Kumar A, Naushad M et al (2021) Adsorptional-photocatalytic removal of fast sulphon black dye by using chitin-cl-poly(itaconic acid-co-acrylamide)/zirconium tungstate nanocomposite hydrogel. J Hazard Mater 416:125714. https://doi.org/10.1016/j.jhazmat.2021.125714

4. Dhaouadi F, Sellaoui L, Chávez-González B et al (2021) Application of a heterogeneous physical model for the adsorption of Cd2+, Ni2+, Zn2+ and Cu2+ ions on flamboyant pods functionalized with citric acid. Chem Eng J 417. https://doi.org/10.1016/j.cej.2020.127975

5. Zhang D, Xu W, Cai J et al (2020) Citric acid-incorporated cellulose nanofibrous mats as food materials-based biosorbent for removal of hexavalent chromium from aqueous solutions. Int J Biol Macromol 149:459–466. https://doi.org/10.1016/j.ijbiomac.2020.01.199

6. Anh NTH, Phuc TT, An TNM et al (2020) Microwave-assisted preparation of magnetic citric acid-sugarcane bagasse for removal of textile dyes. Indones J Chem 20:1101–1109. https://doi.org/10.22146/ijc.48713

7. Msaadi R, Sassi W, Hihn J-Y et al (2022) Valorization of pomegranate peel balls as bioadsorbents of methylene blue in aqueous media. Emergent Mater 5:381–390. https://doi.org/10.1007/s42247-021-00174-w

8. Jithendra Kumara KS, Krishnamurthy G, Walmik P et al (2021) Synthesis of reduced graphene oxide decorated with Sn/Na doped TiO2 nanocomposite: a photocatalyst for Evans blue dye degradation. Emergent Mater 4:457–468. https://doi.org/10.1007/s42247-021-00206-5

9. Zambrano-Intriago LA, Gorozabel-Mendoza ML, Córdova Mosquera A et al (2022) Kinetics, equilibrium, and thermodynamics of the blue 19 dye adsorption process using residual biomass attained from rice cultivation. Biomass Convers Biorefinery 12:3843–3855. https://doi.org/10.1007/s13399-020-00944-2

10. Jiang Z, Ho SH, Wang X et al (2021) Application of biodegradable cellulose-based biomass materials in wastewater treatment. Environ Pollut 290:118087. https://doi.org/10.1016/j.envpol.2021.118087

11. Liu Q, Li Y, Chen H et al (2020) Superior adsorption capacity of functionalised straw adsorbent for dyes and heavy-metal ions. J Hazard Mater 382:121040. https://doi.org/10.1016/j.jhazmat.2019.121040

12. Thomas B, Shilpa EP, Alexander LK (2021) Role of functional groups and morphology on the pH-dependent adsorption of a cationic dye using banana peel, orange peel, and neem leaf bioadsorbents. Emergent Mater 4:1479–1487. https://doi.org/10.1007/s42247-021-00237-y

13. El Khomri M, El Messaoudi N, Dbik A et al (2022) Modification of low-cost adsorbent prepared from agricultural solid waste for the adsorption and desorption of cationic dye. Emergent Mater 5:1679–1688. https://doi.org/10.1007/s42247-022-00390-y

14. Ali A, Saeed K (2016) Phenol removal from aqueous medium using chemically modified banana peels as low-cost adsorbent. Desalin Water Treat 57:11242–11254. https://doi.org/10.1080/19443994.2015.1041057

15. Enaime G, Baçaoui A, Yaacoubi A, Lübken M (2020) Biochar for wastewater treatment—conversion technologies and applications. Appl Sci 10:3492. https://doi.org/10.3390/app10103492

16. Karić N, Maia AS, Teodorović A et al (2022) Bio-waste valorisation: agricultural wastes as biosorbents for removal of (in)organic pollutants in wastewater treatment. Chem Eng J Adv 9. https://doi.org/10.1016/j.ceja.2021.100239

17. Ramrakhiani L, Ghosh S, Majumdar S (2016) Surface modification of naturally available biomass for enhancement of heavy metal removal efficiency, upscaling prospects, and management aspects of spent biosorbents: a review. Appl Biochem Biotechnol 180:41–78. https://doi.org/10.1007/s12010-016-2083-y

18. Nazir H, Salman M, Athar M et al (2019) Citric acid functionalized bougainvillea spectabilis: a novel, sustainable, and cost-effective biosorbent for removal of heavy metal (Pb2+) from waste water. Water Air Soil Pollut 230. https://doi.org/10.1007/s11270-019-4360-1

19. Essekri A, Aarab N, Hsini A et al (2022) Enhanced adsorptive removal of crystal violet dye from aqueous media using citric acid modified red-seaweed: experimental study combined with RSM process optimization. J Dispers Sci Technol 43:1359–1372. https://doi.org/10.1080/01932691.2020.1857263

20. Gupta H, Gogate PR (2016) Intensified removal of copper from waste water using activated watermelon based biosorbent in the presence of ultrasound. Ultrason Sonochem 30:113–122. https://doi.org/10.1016/j.ultsonch.2015.11.016

21. Gong R, Jin Y, Chen F et al (2006) Enhanced malachite green removal from aqueous solution by citric acid modified rice straw. J Hazard Mater 137:865–870. https://doi.org/10.1016/j.jhazmat.2006.03.010

22. Zhu B, Fan T, Zhang D (2008) Adsorption of copper ions from aqueous solution by citric acid modified soybean straw. J Hazard Mater 153:300–308. https://doi.org/10.1016/j.jhazmat.2007.08.050

23. Marshall WE, Wartelle LH, Boler DE et al (1999) Enhanced metal adsorption by soybean hulls modified with citric acid. Bioresour

Technol 69:263–268. https://doi.org/10.1016/S0960-8524(98)00185-0

24. Sajab MS, Chia CH, Zakaria S et al (2011) Citric acid modified kenaf core fibres for removal of methylene blue from aqueous solution. Bioresour Technol 102:7237–7243. https://doi.org/10.1016/j.biortech.2011.05.011

25. Altundoğan HS, Topdemir A, Çakmak M, Bahar N (2016) Hardness removal from waters by using citric acid modified pine cone. J Taiwan Inst Chem Eng 58:219–225. https://doi.org/10.1016/j.jtice.2015.07.002

26. Gong R, Zhu S, Zhang D et al (2008) Adsorption behavior of cationic dyes on citric acid esterifying wheat straw: kinetic and thermodynamic profile. Desalination 230:220–228. https://doi.org/10.1016/j.desal.2007.12.002

27. Wang P, Ma Q, Hu D, Wang L (2016) Adsorption of methylene blue by a low-cost biosorbent: citric acid modified peanut shell. Desalin Water Treat 57:10261–10269. https://doi.org/10.1080/19443994.2015.1033651

28. Leyva-Ramos R, Landin-Rodriguez LE, Leyva-Ramos S, Medellin-Castillo NA (2012) Modification of corncob with citric acid to enhance its capacity for adsorbing cadmium(II) from water solution. Chem Eng J 180:113–120. https://doi.org/10.1016/j.cej.2011.11.021

29. Zhou Y, Zhang R, Gu X, Lu J (2015) Adsorption of divalent heavy metal ions from aqueous solution by citric acid modified pine sawdust. Sep Sci Technol 50:245–252. https://doi.org/10.1080/01496395.2014.956223

30. Ramana DKV, Reddy DHK, Kumar BN et al (2012) Removal of nickel from aqueous solutions by citric acid modified Ceiba pentandra hulls: equilibrium and kinetic studies. Can J Chem Eng 90:111–119. https://doi.org/10.1002/cjce.20565

31. Cerino-Córdova FJ, Díaz-Flores PE, García-Reyes RB et al (2013) Biosorption of Cu(II) and Pb(II) from aqueous solutions by chemically modified spent coffee grains. Int J Environ Sci Technol 10:611–622. https://doi.org/10.1007/s13762-013-0198-z

32. Bessashia W, Berredjem Y, Hattab Z, Bououdina M (2020) Removal of Basic Fuchsin from water by using mussel powdered eggshell membrane as novel bioadsorbent: equilibrium, kinetics, and thermodynamic studies. Environ Res 186:109484. https://doi.org/10.1016/j.envres.2020.109484

33. Sharma S, Sharma G, Kumar A et al (2022) Adsorption of cationic dyes onto carrageenan and itaconic acid-based superabsorbent hydrogel: synthesis, characterization and isotherm analysis. J Hazard Mater 421:126729. https://doi.org/10.1016/j.jhazmat.2021.126729

34. Ait Ahsaine H, Zbair M, Anfar Z et al (2018) Cationic dyes adsorption onto high surface area 'almond shell' activated carbon: kinetics, equilibrium isotherms and surface statistical modeling. Mater Today Chem 8:121–132. https://doi.org/10.1016/j.mtchem.2018.03.004

35. El Haddad M (2016) Removal of Basic Fuchsin dye from water using mussel shell biomass waste as an adsorbent: equilibrium, kinetics, and thermodynamics. J Taibah Univ Sci 10:664–674. https://doi.org/10.1016/j.jtusci.2015.08.007

36. Kalita S, Pathak M, Devi G et al (2017) Utilization of: Euryale ferox Salisbury seed shell for removal of basic fuchsin dye from water: equilibrium and kinetics investigation. RSC Adv 7:27248–27259. https://doi.org/10.1039/c7ra03014b

37. Apostol I, Anghel N, Doroftei F et al (2023) Xanthan or esterified xanthan/cobalt ferrite-lignin hybrid materials for methyl blue and basic fuchsine dyes removal: equilibrium, kinetic and thermodynamic studies. Mater Today Chem 27:101299. https://doi.org/10.1016/j.mtchem.2022.101299

38. Wang N, Qiu Y, Hu K et al (2021) One-step synthesis of cake-like biosorbents from plant biomass for the effective removal and recovery heavy metals: effect of plant species and roles of

39. xanthation. Chemosphere 266:129129. https://doi.org/10.1016/j.chemosphere.2020.129129

39. Zafar S, Khan MI, Lashari MH et al (2020) Removal of copper ions from aqueous solution using NaOH-treated rice husk. Emergent Mater 3:857–870. https://doi.org/10.1007/s42247-020-00126-w

40. Radwan EK, Abdel-Aty AM, El-Wakeel ST, Abdel Ghafar HH (2020) Bioremediation of potentially toxic metal and reactive dye-contaminated water by pristine and modified Chlorella vulgaris. Environ Sci Pollut Res 27:21777–21789. https://doi.org/10.1007/s11356-020-08550-5

41. Kurniawan TA, Chan GYS, Lo W, Babel S (2006) Comparisons of low-cost adsorbents for treating wastewaters laden with heavy metals. Sci Total Environ 366:409–426. https://doi.org/10.1016/j.scitotenv.2005.10.001

42. Kalavathy MH, Regupathi I, Pillai MG, Miranda LR (2009) Modelling, analysis and optimization of adsorption parameters for H3PO4 activated rubber wood sawdust using response surface methodology (RSM). Colloids Surf B Biointerfaces 70:35–45. https://doi.org/10.1016/j.colsurfb.2008.12.007

43. Rahar S, Nagpal N, Swami G et al (2011) Pharmacognostical studies of Saccharum munja Roxb Root. Int J PharmTech Res 3:792–800

44. Lila MK, Komal UK, Singh Y, Singh I (2022) Extraction and characterization of Munja fibers and its potential in the biocomposites. J Nat Fibers 19:2675–2693. https://doi.org/10.1080/15440478.2020.1821287

45. Yadav A, Bagotia N, Yadav S et al (2021) Adsorptive studies on the removal of dyes from single and binary systems using Saccharum munja plant-based novel functionalized CNT composites. Environ Technol Innov 24. https://doi.org/10.1016/j.eti.2021.102015

46. Kumar M, Mishra PK, Upadhyay SN (2019) Pyrolysis of Saccharum munja: optimization of process parameters using response surface methodology (RSM) and evaluation of kinetic parameters. Bioresour Technol Rep 8:100332. https://doi.org/10.1016/j.biteb.2019.100332

47. Neelamegan H, Yang D-K, Lee G-J et al (2020) Synthesis of magnetite nanoparticles anchored cellulose and lignin-based carbon nanotube composites for rapid oil spill cleanup. Mater Today Commun 22:100746. https://doi.org/10.1016/j.mtcomm.2019.100746

48. Zhang H, Zhou J, Muhammad Y et al (2019) Citric acid modified bentonite for congo red adsorption. Front Mater 6:1–11. https://doi.org/10.3389/fmats.2019.00005

49. Soldatkina L, Yanar M (2023) Optimization of adsorption parameters for removal of cationic dyes on lignocellulosic agricultural waste modified by citric acid: central composite design. ChemEng 7. https://doi.org/10.3390/chemengineering7010006

50. Singh S, Prajapati AK, Chakraborty JP, Mondal MK (2023) Adsorption potential of biochar obtained from pyrolysis of raw and torrefied Acacia nilotica towards removal of methylene blue dye from synthetic wastewater. Biomass Convers Biorefinery 13:6083–6104. https://doi.org/10.1007/s13399-021-01645-0

51. Yadav A, Bagotia N, Yadav S et al (2021) Adsorptive studies on the removal of dyes from single and binary systems using Saccharum munja plant-based novel functionalized CNT composites. Environ Technol Innov 24:102015. https://doi.org/10.1016/j.eti.2021.102015

52. Chowdhury S, Chakraborty S, Das P (2013) Adsorption of crystal violet from aqueous solution by citric acid modified rice straw: equilibrium, kinetics, and thermodynamics. Sep Sci Technol 48:1339–1348. https://doi.org/10.1080/01496395.2012.729122

53. Azmi SNH, Al Lawati WM, Al Hoqani UHA et al (2022) Development of a citric-acid-modified cellulose adsorbent derived from Moringa peregrina leaf for adsorptive removal of citalopram HBr

in aqueous solutions. Pharmaceuticals 15. https://doi.org/10.3390/ph15060760

54. Yadav S, Yadav A, Bagotia N et al (2022) Novel composites of Pennisetum glaucum with CNT: preparation, characterization and application for the removal of safranine O and methylene blue dyes from single and binary systems. Biomass Convers Biorefinery. https://doi.org/10.1007/s13399-021-02240-z

55. Alejandra G, Giraldo G, Mantovan J, Marim BM (2021) Surface modification of cellulose from oat hull with citric acid using ultrasonication and reactive extrusion assisted processes. Polysaccharides 2(2):218–233. https://doi.org/10.3390/polysaccharides2020015

56. Kavci E, Erkmen J, Bingöl MS (2023) Removal of methylene blue dye from aqueous solution using citric acid modified apricot stone. Chem Eng Commun 210:165–180. https://doi.org/10.1080/00986445.2021.2009812

57. Chadha R, Saini A, Arora P et al (2012) Cocrystals of efavirenz with selected conformers: preparation and characterization. Int J Pharm Pharm Sci 4:244–250

58. Reda S (2011) Evaluation of antioxidants stability by thermal analysis and its protective effect in heated edible vegetable oil. Food Sci Technol 31:475–480. https://doi.org/10.1590/S0101-20612011000200030

59. Murigi MK, Madivoli ES, Mathenyu MM et al (2014) Comparison of physicochemical characteristics of microcrystalline cellulose from four abundant Kenyan biomasses. IOSR J Polym Text Eng 1:53–63. https://doi.org/10.9790/019x-0125363

60. Sadri Moghaddam S, Alavi Moghaddam MR, Arami M (2010) Coagulation/flocculation process for dye removal using sludge from water treatment plant: Optimization through response surface methodology. J Hazard Mater 175:651–657. https://doi.org/10.1016/j.jhazmat.2009.10.058

61. Okolo BI, Oke EO, Agu CM et al (2020) Adsorption of lead(II) from aqueous solution using Africa elemi seed, mucuna shell and oyster shell as adsorbents and optimization using Box–Behnken design. Appl Water Sci 10. https://doi.org/10.1007/s13201-020-01242-y

62. Yadav A, Bagotia N, Yadav S et al (2022) In-situ fabrication of surfactant modified CNT-based novel bio-composite and its performance evaluation for simultaneous removal of anionic dyes: Optimization by Box-Behnken design. Sep Purif Technol 284. https://doi.org/10.1016/j.seppur.2021.120262

63. Hatiya NA, Reshad AS, Negie ZW (2022) Chemical modification of neem (Azadirachta indica) biomass as bioadsorbent for removal of Pb2+ion from aqueous waste water. Adsorpt Sci Technol 2022. https://doi.org/10.1155/2022/7813513

64. Jawad AH, Malek NNA, Abdulhameed AS, Razuan R (2020) Synthesis of magnetic chitosan-fly Ash/Fe3O4 composite for adsorption of reactive orange 16 dye: optimization by Box–Behnken design. J Polym Environ 28:1068–1082. https://doi.org/10.1007/s10924-020-01669-z

65. Ba Mohammed B, Hsini A, Abdellaoui Y et al (2020) Fe-ZSM-5 zeolite for efficient removal of basic Fuchsin dye from aqueous solutions: synthesis, characterization and adsorption process optimization using BBD-RSM modeling. J Environ Chem Eng 8. https://doi.org/10.1016/j.jece.2020.104419

66. Sulyman M, Kucinska-Lipka J, Sienkiewicz M, Gierak A (2021) Development, characterization and evaluation of composite adsorbent for the adsorption of crystal violet from aqueous solution: isotherm, kinetics, and thermodynamic studies. Arab J Chem 14:103115. https://doi.org/10.1016/j.arabjc.2021.103115

67. Pandey D, Daverey A, Dutta K et al (2022) Valorization of waste pine needle biomass into biosorbents for the removal of methylene blue dye from water: kinetics, equilibrium and thermodynamics study. Environ Technol Innov 25:102200. https://doi.org/10.1016/j.eti.2021.102200

68. Zheng X, Ni C, Xiao W et al (2022) Ionic liquid grafted polyethersulfone nanofibrous membrane as recyclable adsorbent with simultaneous dye, heavy metal removal and antibacterial property. Chem Eng J 428:132111. https://doi.org/10.1016/j.cej.2021.132111

69. Sarma GK, Sen Gupta S, Bhattacharyya KG (2019) Removal of hazardous basic dyes from aqueous solution by adsorption onto kaolinite and acid-treated kaolinite: kinetics, isotherm and mechanistic study. SN Appl Sci 1:1–15. https://doi.org/10.1007/s42452-019-0216-y

70. Bello OS, Ahmad MA (2012) Coconut (Cocos nucifera) shell based activated carbon for the removal of malachite green dye from aqueous solutions. Sep Sci Technol 47:903–912. https://doi.org/10.1080/01496395.2011.630335

71. Jabar JM, Odusote YA (2021) Utilization of prepared activated biochar from water lily (Nymphaea lotus) stem for adsorption of malachite green dye from aqueous solution. Biomass Convers Biorefinery. https://doi.org/10.1007/s13399-021-01399-9

72. Chowdhury S, Mishra R, Saha P, Kushwaha P (2011) Adsorption thermodynamics, kinetics and isosteric heat of adsorption of malachite green onto chemically modified rice husk. Desalination 265:159–168. https://doi.org/10.1016/j.desal.2010.07.047

73. Hoslett J, Ghazal H, Ahmad D, Jouhara H (2019) Removal of copper ions from aqueous solution using low temperature biochar derived from the pyrolysis of municipal solid waste. Sci Total Environ 673:777–789. https://doi.org/10.1016/j.scitotenv.2019.04.085

74. Oyelude EO, Frimpong F, Dawson D (2015) Studies on the removal of basic fuchsin dye from aqueous solution by HCl treated malted sorghum mash. J Mater Environ Sci 6:1126–1136

75. Šćiban M, Klašnja M, Škrbić B (2008) Adsorption of copper ions from water by modified agricultural by-products. Desalination 229:170–180. https://doi.org/10.1016/j.desal.2007.08.017

76. Basci N, Kocadagistan E, Kocadagistan B (2004) Biosorption of copper (II) from aqueous solutions by wheat shell. Desalination 164:135–140. https://doi.org/10.1016/S0011-9164(04)00172-9

77. Yamil YL, Georgin J, dos Reis GS et al (2020) Utilization of Pacara Earpod tree (Enterolobium contortisilquum) and Ironwood (Caesalpinia leiostachya) seeds as low-cost biosorbents for removal of basic fuchsin. Environ Sci Pollut Res 27:33307–33320. https://doi.org/10.1007/s11356-020-09471-z

78. Grassi P, Georgin J, S. P. Franco D et al (2023) Removal of dyes from water using Citrullus lanatus seed powder in continuous and discontinuous systems. Int J Phytoremediation 1–16. https://doi.org/10.1080/15226514.2023.2225615

79. Tahir N, Bhatti HN, Iqbal M, Noreen S (2017) Biopolymers composites with peanut hull waste biomass and application for Crystal Violet adsorption. Int J Biol Macromol 94:210–220. https://doi.org/10.1016/j.ijbiomac.2016.10.013

80. Chakraborty S, Chowdhury S, Das P (2012) Insight into biosorption equilibrium, kinetics and thermodynamics of crystal violet onto Ananas comosus (pineapple) leaf powder. Appl Water Sci 2:135–141. https://doi.org/10.1007/s13201-012-0030-9

81. Essekri A, Hsini A, Naciri Y et al (2021) Novel citric acid-functionalized brown algae with a high removal efficiency of crystal violet dye from colored wastewaters: insights into equilibrium, adsorption mechanism, and reusability. Int J Phytoremediation 23:336–346. https://doi.org/10.1080/15226514.2020.1813686

82. Essekri A, Laabd M, Fatni A et al (2023) The use of raw and modified acacia leaves for adsorptive removal of crystal violet from water. Chem Eng Res Des 190:143–156. https://doi.org/10.1016/j.cherd.2022.12.010

83. Essekri A, Haki MA, Laabd M et al (2023) Citric acid-functionalized Acacia pods as a robust biosorbent for decontamination of wastewater containing crystal violet dye: Experimental study combined with statistical optimization. Chem Eng Res Des 195:390–403. https://doi.org/10.1016/j.cherd.2023.05.044

84. Low KS, Lee CK, Leo AC (1995) Removal of metals from electroplating wastes using banana pith. Bioresour Technol 51:227–231. https://doi.org/10.1016/0960-8524(94)00123-I

85. Acar FN, Eren Z (2006) Removal of Cu(II) ions by activated poplar sawdust (Samsun Clone) from aqueous solutions. J Hazard Mater 137:909–914. https://doi.org/10.1016/j.jhazmat.2006.03.014